Sea surface chlorophyll signature in the tropical Pacific during eastern and central Pacific ENSO events

Marie-Hélène Radenac, Fabien Léger, Awnesh Singh, Thierry Delcroix

Sea surface chlorophyll signature in the tropical Pacific during Eastern and Central Pacific ENSO events

Marie-Hélène Radenac[(*)], Fabien Léger, Awnesh Singh, and Thierry Delcroix

LEGOS

UMR 5566 CNRS/IRD/CNES/UPS

14 avenue Edouard Belin

31400 Toulouse

France

[(*)] corresponding author: Marie-Hélène Radenac, IRD/LEGOS, UMR 5566, 14 avenue Edouard Belin, 31400 Toulouse, France (marie-helene.radenac@legos.obs-mip.fr)

Submitted to J. Geophys. Res. (2011JC007841). Revised version

7 February 2012

Abstract

Recent analyses of physical measurements show the existence of a Central Pacific type of El Niño (CPEN) with a sea surface temperature warming pattern distinct from that of the "classical" Eastern Pacific El Niño (EPEN). In this study, we analyze the surface chlorophyll signature of El Niño-Southern Oscillation (ENSO), using monthly maps of satellite-derived chlorophyll anomalies between September 1997 and December 2010. We identify five typical ENSO structures. The first structure describes the lonely 1997-1998 EPEN of the period, the second and third represent La Niña, the fourth illustrates intermediate conditions, and the fifth characterizes CPEN. During the 1997-1998 EPEN, a large eastward shift of the oligotrophic warm pool and a reduction of equatorial upwelling result in negative chlorophyll anomalies east of 170°E between 10°S and 10°N. During the four CPEN events, a reduced eastward shift yields negative chlorophyll anomalies in the equatorial band, within about 160°E and 160°W only. Westward surface current in the central basin limits the expansion of the anomaly core. Negative chlorophyll anomalies that extend eastward from the equatorial anomaly core probably result from reduced upward iron fluxes linked to the deepening of the Equatorial Undercurrent. During La Niña, the westward expansion of the equatorial upwelling results in positive chlorophyll anomalies west of the date line. Away from the equatorial band, advection of oligotrophic warm pool waters by enhanced eastward countercurrents drives negative anomalies within 8-10°N and towards the Marquesas Islands during CPEN, while reduced countercurrents leads to positive chlorophyll anomaly during La Niña.

1. Introduction

It is now well established that El Niño-Southern Oscillation (ENSO) events account for an important part of the global climate variability on interannual timescales with notable impacts on environment, ecosystems, economy, and society [Glantz, 2000; McPhaden et al., 2006]. Numerous studies have shown that sea surface temperatures (SST) warmer than seasonal values invade the central and, sometimes, the eastern equatorial Pacific during the warm phase (El Niño) of the ENSO cycle. However, many differences have been observed amongst the various El Niño events. Among those differences, warm SST anomalies occur both in the eastern and central Pacific during the conventional El Niño, also referred to as canonical, cold tongue, or eastern Pacific El Niño, whilst warm SST anomalies remain confined only in the central Pacific during most of the events observed in recent years [Trenberth and Stepaniak, 2001; Ashok et al., 2007; Kug et al., 2009; Kao and Yu, 2009]. Interestingly, this later type of events, referred to as central Pacific El Niño, dateline El Niño, or El Niño Modoki, has been shown to be more intense in recent decades [Lee and McPhaden, 2010] and could be more frequent in a warming world [Yeh et al., 2009]. Some studies argue that this later type of events differs from conventional ENSO [Ashok et al., 2007] while other studies argue that both types belong to an overall nonlinear phenomenon [Takahashi et al., 2011]. In this study, we will refer to these two types of El Niño as Eastern Pacific (EP) and Central Pacific (CP) El Niño.

Based on atmospheric observations, the well known Southern Oscillation Index (SOI) is often used to identify the warm and cold phases of ENSO. Based on oceanic observations, several SST indices were further proposed to distinguish the EP and CP El Niño. These mainly rely on comparisons between SST anomalies, normalized or not, in the Niño3 (5°S-5°N, 150°W-90°W) and Niño4 (5°S-5°N, 160°E-150°W) regions [Kug et al., 2009; Yeh et al., 2009; Kim

et al., 2009]. Some studies also rely on other possible El Niño indices such as the Trans-Niño Index [TNI; Trenberth and Stepaniak, 2001], El Niño Modoki Index [EMI; Ashok et al., 2007], and other metrics [e.g. Kao and Yu, 2009; Takahashi et al., 2011; Ren and Jin, 2011]. Singh et al. [2011] also proposed ENSO indices based on differences of sea surface salinity (SSS) anomaly in two equatorial regions and in the South Pacific Convergence Zone (SPCZ). Identifications of EP and CP events following several of these methods are fairly consistent. Some discrepancies however exist and reflect the complexity of the problem as events may evolve from one type to the other [Yu and Kim, 2010; Takahashi et al., 2011] or may have patterns intermediate between the EP and CP types [Kug et al., 2009]. Table 1 summarizes the classification of EP and CP ENSO events since the strong El Niño in 1997-1998 (see also Table 1 in Singh et al. [2011] for previous years).

Although physical processes responsible for SST anomaly patterns during CP El Niño are, by far, not completely understood, they seem to differ from the ones leading to EP El Niño. Basically, during EP El Niño, the weakening of the trade winds and basin wide variations of thermocline depth lead to warming in the eastern equatorial Pacific while positive SST anomalies in the central basin result from eastward advection of the warm pool [Picaut et al., 2001; Vialard et al., 2001; Kao and Yu, 2009; Kug et al., 2009]. For CP El Niño, local atmospheric forcing and zonal advection are likely mechanisms involved in the development, confinement, and decay of anomalies in the central basin [Kao and Yu, 2009; Kug et al., 2009; Singh et al., 2011]. The so-called thermocline and advection feedbacks would then be at work during EP El Niño, while the advection feedback would mostly be at work during CP El Niño.

Mechanisms that control the SST warming during EP El Niño apparently account for the decrease of biological production in the equatorial Pacific. During the 1997-1998 El Niño, nutrient- and phytoplankton-poor (surface chlorophyll lower than 0.1 mg m^{-3}) waters of the warm pool were advected eastward to the central and eastern basins while vertical inputs of nutrients decreased in the east because of the thermocline deepening and the reduction of the upward vertical velocity [Chavez et al., 1998; Radenac et al., 2001]. The ecosystem of the equatorial upwelling region is iron-limited [Landry et al., 1997] and the thermocline deepening is associated with the depression of the Equatorial Undercurrent (EUC) that transports iron across the basin from the western Pacific [Gordon et al., 1997; Wells et al., 1999; Lacan and Jeandel, 2001]. As biologically available iron in the photic layer is mainly upwelled from the EUC [Gordon et al., 1997], strong reduction of the iron fluxes ensues from the depression of the EUC during El Niño [Barber et al., 1996; Gordon et al., 1997; Chavez et al., 1999; Friedrichs and Hofmann, 2001]. The result is a collapse of new and primary production in the equatorial Pacific during the 1997-1998 [Chavez et al., 1999; Strutton and Chavez, 2000; Radenac et al., 2001; Turk et al., 2001] and previous EP El Niño events [Barber and Kogelschatz, 1990; Barber et al., 1996]. However, to our knowledge, no study characterizes the response of the equatorial ecosystems to the subsequent CP El Niño events in 2002-2003, 2004-2005, 2006-2007, and 2009-2010, apart from the recent paper by Turk et al. [2011]. This is the goal of this study. The occurrence and strength of CP El Niño have increased since the 1990s (Lee and McPhaden, 2010) and their frequency may still increase in future as stressed by Yeh et al. (2009). Therefore, further investigations are necessary to better understand ENSO related physical-biological interactions and their impacts on biological fields and dynamics up to top predators.

120 The manuscript is organized as follows. Section 2 describes the satellite-derived data that
121 allow us to describe the 1997-2010 changes in surface chlorophyll on basin scale. To set the
122 context, section 3 compares the SST, SSS, and surface chlorophyll anomalies in the equatorial
123 band. Then, section 4 contrasts the surface chlorophyll anomaly signatures characterizing the
124 EP and CP El Niño, and section 5 analyzes the possible impacts of changes in surface
125 circulation and thermocline depth on the surface chlorophyll distribution. A discussion and
126 conclusion appear in the last section.
127
128 **2. Data and methods**
129 Surface chlorophyll concentrations were derived from Sea-viewing Wide Field-of-view
130 Sensor (SeaWiFS) measurements and from the Moderate Resolution Imaging
131 Spectroradiometer (MODIS) measurements aboard the Aqua satellite. SeaWiFS data are
132 available between September 1997 and December 2010 and MODIS data since July 2002. We
133 used 9 km resolution monthly composites computed by the NASA Goddard Space Flight
134 Center (GSFC) Distributed Active Archive Center (DAAC) [McClain et al., 2004]. When a
135 SeaWiFS monthly map was not available or had less than 60% of data available (7 maps, i.e.
136 4.4% of the time), we used the Aqua MODIS map in order to obtain a complete chlorophyll
137 time series from September 1997 to December 2010. For each location, chlorophyll values
138 higher than 3 mg m^{-3} and/or that were more than five standard deviations away from the
139 1997-2010 mean were treated as missing (Messié and Radenac, 2006). In the calculations, we
140 interpolated the data onto a 1°×1° grid following the method of Yoder and Kennelly [2003].
141 First, we computed 0.25°×0.25° maps using the maximum likelihood estimator [Campell et
142 al., 1995]. Then, most of the data gaps due to sparse clouds were filled by taking the median
143 of every 1°×1° cell. The remaining missing data were filled by taking the median of the first
144 neighbors. The chlorophyll anomalies we present are relative to a mean seasonal cycle

145 calculated between 1998 and 2010. We also used monthly maps of Photosynthetically
146 Available Radiation (PAR) estimates derived from SeaWiFS and MODIS [Frouin et al.,
147 2003].
148
149 SST data was provided by the Hadley Centre for Climate Prediction and Research Sea Ice and
150 Sea Surface Temperature HadISST1 dataset [Rayner et al., 2003]. Monthly SST maps are
151 available since 1870 on a 1°×1° grid. SSS data came from the recently-updated Delcroix et al.
152 [2011] product for the tropical Pacific. Monthly SSS data are available on a 1°×1° grid and
153 span from 1950 to 2009. Monthly near surface currents were obtained from the Ocean Surface
154 Current Analysis - Real time (OSCAR) 1°×1° product; the geostrophic, wind-driven, and
155 thermal-wind components of which are derived from satellite data [Bonjean and Lagerloef,
156 2002]. Monthly anomalies of wind speed and depth of the 20°C ($Z_{20°C}$) isotherms are derived
157 from time series recorded at the Tropical Atmosphere Ocean/Triangle Trans Ocean Buoy
158 Network [TAO/TRITON; McPhaden et al., 1998] moorings. We also used time series of the
159 SOI and EMI [Ashok et al., 2007].
160
161 Different statistical procedures have been used in the literature to discriminate ENSO features.
162 To name a few, these include regression of anomaly onto specific ENSO indices [Trenberth
163 and Stepaniak, 2001; Ren and Jin, 2011; Takahashi et al., 2011; Singh and Delcroix, 2011],
164 Empirical Orthogonal Functions (EOF) analyses [Ashok et al., 2007; Park et al., 2011],
165 combined regression-EOF analyses [Kao and Yu, 2009], neural network [Hsieh, 2001; Leloup
166 et al., 2007], and Agglomerative Hierarchical Clustering (AHC) analysis [Kao and Yu, 2009;
167 Singh et al., 2011]. We tested here the EOF and AHC analyses on chlorophyll in the tropical
168 Pacific. The EOF analysis of the chlorophyll anomaly indicates that the CP El Niño signal is
169 distributed over at least the first, third, and fourth modes (not shown). Hence, the EOF

technique does not distinguish properly EP and CP El Niño. A similar leakage of the signal was found for the EOF analysis of SSS in the tropical Pacific [Singh et al., 2011]. Therefore, we chose to perform an AHC analysis on the monthly surface chlorophyll anomalies to characterize ENSO related signatures. In this nonlinear composite procedure, maps are merged into clusters according to their similarity, estimated from the smallest Euclidean distance (defined as the root-mean-squared distance between each pairs of maps). The clustering procedure can be represented by a dendrogram tree that illustrates combinations made at each successive step of the analysis. This technique has been successfully performed on SST [Kao and Yu, 2009], SSS [Singh et al., 2011], and South Pacific Convergence Zone (SPCZ) location [Vincent et al., 2009] to separate ENSO signatures in the tropical Pacific. In this study, we applied the AHC method to monthly maps of surface chlorophyll anomalies for the region between 130°E-70°W and 10°S-10°N. The Indonesian Throughflow region and Central and South America coastal upwellings were excluded as regional effects may mask the basin-scale ENSO signature (Fig. 1).

3. Comparing SST, SSS, and surface chlorophyll anomalies in the equatorial band

The mean chlorophyll distribution and its interannual variability are presented first to set the context (Fig. 1). The mean values were computed by averaging all monthly values covering the 1997-2010 period, and the interannual variability was defined as the standard deviation of the chlorophyll anomalies (relative to the mean seasonal cycle). Figure 1a shows that the mean chlorophyll is lower than 0.3 mg m^{-3} outside the Central and South America upwelling regions, with well-marked maxima in a huge equatorial region spreading westward from the South American coast. These values are mostly due to the equatorial upwelling which brings cool, salty, and nutrient-rich waters toward the surface. Although the surface nitrate concentration is high in the upwelling, the chlorophyll content remains moderate (less than

195 0.2 mg m^{-3} on average) because of an iron-limited and grazing-balanced ecosystem [Landry et
196 al., 1997]. Mesotrophic waters of the equatorial upwelling are surrounded by oligotrophic
197 waters ([chl] < 0.1 mg m^{-3}) of the warm pool to the west and of subtropical gyres poleward
198 (note also the moderate mesotrophic waters north of Papua New Guinea and near the
199 Solomon Sea). The interannual variability (Fig. 1b) is high between 10°S and 10°N,
200 especially along the equator, in the North Equatorial Countercurrent (NECC) region, around
201 Papua New Guinea, and in the Central and South America coastal upwelling regions.
202
203 Looking at the regions of maximum interannual variability, the longitude-time distributions of
204 the 5°N-5°S averaged SST, SSS, and surface chlorophyll anomalies are shown in figure 2. For
205 all El Niño events, the maximum positive SST anomaly occurs during boreal winter, between
206 September and February (Fig. 2a). The location and amplitude of the anomaly differ from one
207 event to the other. The 1997-1998 (EP, see Table 1 and below) El Niño is the only one with
208 very warm SST anomaly (SSTA > 3°C) that peaks east of 120°W and extends toward the
209 central basin. During the following (CP, see Table 1 and below) El Niño events, the
210 maximum SST anomaly is lower (sometimes less than 1°C) and mostly situated in the central-
211 western basin, at least in 2002-2003, 2004-2005, and 2009-2010. The strongest warming (SST
212 anomaly close to 2° C) during a CP El Niño event is reached during the mature phase of the
213 2009-2010 event, in agreement with Lee and McPhaden [2010].
214
215 The strongest negative SSS anomalies (Fig. 2b) appear to be located west of the maximum
216 positive SST anomalies. During the 1997-1998 EP El Niño, the SSS anomaly is negative east
217 of 160°E, with a maximum freshening near the date line. During the following CP El Niño
218 events, the maximum negative anomalies tend to be displaced westward by 10 to 15° of
219 longitude, except in 2002-2003, in agreement with Singh et al (2011).

The time series of surface chlorophyll anomaly (Fig. 2c) is reminiscent of the SSS anomaly time series as strong negative chlorophyll anomalies tend to be located west of the warm El Niño-related SST anomalies. In 1997-1998, the strong anomaly core (< -0.12 mg m^{-3}) is near 150°W and the surface chlorophyll concentration is below the mean seasonal value from 150°E to the American coast. During the following events, the negative anomaly core (-0.08 to -0.10 mg m^{-3}) is located in the central-western basin, between about 150°E and 180°, while the moderate anomalies observed eastward range between less than -0.02 mg m^{-3} in 2002-2003 and 2004-2005 to -0.04 mg m^{-3} in 2006-2007 and 2009-2010.

Oligotrophic waters ([chl] < 0.1 mg m^{-3}) have been shown to be quasi-persistent in the eastern part of the equatorial warm pool while moderate mesotrophic waters (surface chlorophyll concentration slightly higher than 0.1 mg m^{-3}) were often observed in its western part [Radenac et al., 2010]. This oligotophic region is delimited by the black contour in Figures 2a, b, c. The easternmost limit of this zone characterizes the eastern edge of the warm pool [Murtugudde et al., 1999; Stoens et al., 1999; Radenac et al., 2010] that separates waters of the eastern warm pool ([chl] < 0.1 mg m^{-3}) from upwelled waters ([chl] > 0.1 mg m^{-3}). Large zonal displacements of the eastern edge of the warm pool occur at interannual timescales and its longitudinal position is related to the phases of ENSO [Picaut and Delcroix, 1995; Le Borgne et al., 2002]. It reaches 130°W during the 1997-1998 EP El Niño and lies between the dateline and 160°W during CP events. Interestingly, the oligotrophic waters of the eastern part of the warm pool follow these movements (Fig. 2c). Thus, the maximum negative chlorophyll and SSS anomaly cores are both located west of the warmest SST anomalies.

Several La Niña years interleave between El Niño years (Table 1). When La Niña events reach their mature phase in boreal winter (e.g. in early 2008), SST in the central and eastern basins are cooler while becoming slightly warmer west of 160°E (Fig. 2a). Strong positive anomalies of SSS and surface chlorophyll are closely related west of 150°W (Figs. 2b, c). They are located at the western limit of the cool SST anomaly, in the region of zonal displacements of the eastern edge of the warm pool. Chlorophyll anomalies exceed 0.10 mg m^{-3} in 2010 and range between 0.05 and 0.08 mg m^{-3} during the other La Niña years. A moderate increase of chlorophyll (< 0.03 mg m^{-3}) is observed eastward of these maxima.

Figure 2c shows that the chlorophyll anomalies are negative all along the equator in 1997-1998 while the core of chlorophyll anomaly remains west of 150°W during the following boreal winters (see also spatial patterns from the cluster analysis below). Therefore, comparing the chlorophyll anomalies averaged over the Niño3 and Niño4 regions during the peak period of the events (September-February; Fig. 3) mostly concurs with the classification of La Niña and CP and EP El Niño events. Chlorophyll anomalies are negative in both regions during El Niño years (SOI < 0) and positive during La Niña years (SOI > 0). Also, differences between the anomalies in each region are consistent with the CP El Niño as depicted by the EMI (Fig. 3). The amplitude of the chlorophyll anomaly indeed tends to be greater in Niño4 than in Niño3 during CP El Niño (EMI > 0). Following these results, the 2006-2007 El Niño is identified here as a CP event as in the SSS study [Singh et al., 2011] and in contrast to most of the SST studies (Table 1). The 2009-2010 event, acknowledged as the warmest CP El Niño during the last decades [Lee and McPhaden, 2010], yields chlorophyll anomalies in Niño4 weaker than during the 2002-2003 event. Actually, the magnitude of the chlorophyll decrease in Niño4 is linked to the eastward expansion of the oligotrophic warm pool (Fig. 2c) whereas warming in Niño4 is not (Fig. 2a). During La Niña

winters, the chlorophyll anomaly in Niño4 is always larger than in Niño3 (except in 1998-1999), suggesting that the strongest increase of chlorophyll occur in the region of zonal shifts of the eastern edge of the warm pool. The greatest winter increase reached in the Niño4 region is in 2010-2011.

4. Describing the spatial patterns of ENSO-related surface chlorophyll anomalies

Using the AHC analysis described in section 2, we identified five clusters out of 160 monthly maps during the September 1997-December 2010 period. As detailed below, we believe they are representative of EP El Niño, equatorial recovery, La Niña, intermediate CP El Niño, and CP El Niño conditions. They occur about 6%, 6%, 34%, 28%, and 26% of the time, respectively. The associated time series and the derived composite maps are presented in figure 4. Occurrences of EP El Niño (1997-1998), CP El Niño (2002-2003, 2004-2005, 2006-2007, 2009-2010), and La Niña events (1998-1999, 1999-2000, 2000-2001, 2007-2008, 2008-2009, 2010-2011) are consistent with those found in previous studies using SST or SSS indices (Table 1) and with the comparison of chlorophyll anomalies in the Niño3 and Niño4 regions (Fig. 3). Of note, the cluster analysis does not classify the end of 1998 as typical La Nina conditions although that period has been described as a La Niña year from the surface chlorophyll distribution [Murtugudde et al., 1999; Radenac et al., 2001; Ryan et al., 2002] and from other variables (Fig. 3; Table 1): the reason for this is discussed below. Intermediate CP El Niño periods occur in 2001-2002, 2003-2004, 2005-2006, and 2007 near CP El Niño years when the SOI or EMI is weak (Fig. 3).

Aside from the "all-month" AHC analysis we present, we also performed an AHC analysis using September to February months only (not shown) because CP and EP El Niño and La Niña events reach their mature phase in boreal winter for most climate variables [Kao and Yu,

294 2009] and for chlorophyll changes [Chavez et al., 1999; Strutton and Chavez, 2000; Radenac
295 et al., 2001; see also Figure 2]. In that case, we obtained similar patterns for the CP and EP El
296 Niño, and La Niña clusters. The strong equatorial signal (Fig. 4c) however did not show up as
297 elevated chlorophyll concentration along the equator was observed in boreal spring and
298 summer. Caution is thus required when selecting some months per year only in analyzing
299 ENSO features.
300
301 Cluster 1 captures the spatial pattern of the only EP El Niño event over the study period (Fig.
302 4b). Given the strength of this event, it is not surprising that its spatial pattern resembles that
303 of the EOF analysis performed on the 1997-1999 chlorophyll data [Wilson and Adamec,
304 2001]. The chlorophyll anomaly is negative over a broad region from 170°E to the American
305 coast and maximum along the equator. The northern limit of the negative anomaly region is
306 sharp and almost zonally oriented near 8°N while the southern limit may look smoother and
307 extends south of 10°S (except west of the dateline). Unlike the SST anomaly pattern during
308 EP El Niño, which is strongest near the American coast and extends westward along the
309 equator [Rasmusson and Carpenter, 1982; Kao and Yu, 2009; Kug et al., 2009], the
310 chlorophyll anomaly seems to have two distinct cores (lower than -0.075 mg m^{-3}). One core is
311 found between the date line and 140°W and the other one east of 110°W in the equatorial
312 region. The chlorophyll anomaly is positive in the western basin mostly between the equator
313 and 10°latitudes.
314
315 Characteristics of surface chlorophyll during the four CP El Niño events are represented by
316 cluster 5 (Fig. 4f). The negative anomaly pattern has an arrow shape whose head would be the
317 core of the largest negative anomaly (less than -0.08 mg m^{-3}) located at the equator around
318 170°E. Thin bands of negative chlorophyll anomaly (-0.02 to -0.01 mg m^{-3}) stretches from the

anomaly core along 8-10°N to the Central American coast, while another of lower magnitude extends to the Marquesas Islands at 140°W, 10°S. The tail of the arrow would be the narrow band of moderate negative anomaly (-0.03 to -0.02 mg m^{-3}) along the equator from the anomaly core to the American coast. The core of maximum negative surface chlorophyll anomaly matches the core of maximum negative SSS anomaly [Singh et al., 2011] during both El Niño types, and in the same way as the SST anomaly, it is shifted westwards during CP El Niño compared to EP El Niño. The three zonal bands of moderate negative chlorophyll anomaly that stretch eastward from the equatorial minimum anomaly core are specific to the chlorophyll signature. In the western Pacific, north of Papua New Guinea and Solomon Islands, chlorophyll anomalies are positive during CP El Niño events.

The timing of La Niña years, captured by cluster 3 (Fig. 4a), are consistent with the occurrence of positive SOI (Fig. 3). The La Nina patterns (Fig. 4d) somewhat mirror the CP El Nino patterns (Fig. 4f) in the western half of the basin, although the maximum anomaly is stronger and extends 5° to 10° longitude further to the west during La Niña. In agreement with figure 3, cluster 3 thus shows that the positive chlorophyll anomalies in Niño4 region are larger than in Niño3 (Fig. 4d). Narrow bands of positive anomaly stretch from the high positive anomaly core along the equator and 6°N -7°N toward the American coast and to the Marquesas Islands. Cluster 2 captures a strong enhancement of the surface chlorophyll concentration (> 0.05 mg m^{-3}) in a narrow equatorial band by the end of 1998 and mid-2010 (Fig. 4a, c) during the strong La Nina events that followed the strong 1997-1998 EP El Niño and 2009-2010 CP El Niño. Two cores with chlorophyll anomaly higher than 0.08 mg m^{-3} are located west of the Kiribati Islands (175°E) and between 140°W and 120°W. Anomalies are negative between 10°S and 10°N in the western basin and poleward of 5° in the east.

Surface chlorophyll distribution captured by cluster 4 (Fig. 4a, e) appears when the SOI and chlorophyll anomalies in the Niño3 and Niño4 regions are weak (Fig. 2). The main feature is a negative anomaly zone in the western equatorial basin.

5. Analyzing possible drivers of surface chlorophyll changes during El Niño events

In this section, we investigate mechanisms that could possibly constrain the overall spatial structure of surface chlorophyll anomaly during El Niño events, relying on changes in surface zonal current, wind, and thermocline depth (assumed to be the 20°C isotherm depth, $Z_{20°C}$). We first recall the main results obtained for the 1997-1998 EP El Niño [Chavez et al., 1999; Murtugudde et al., 1999; Stoens et al., 1999; Wilson and Adamec, 2001; Strutton and Chavez, 2000; Radenac et al., 2001; 2005]. Then, we choose to describe the spatial evolution of chlorophyll anomaly during CP El Niño, with a slight focus on the fairly representative 2002-2003 event, rather than on a composite, in order to preserve tiny structures whose positions are slightly different among events. Figure 5 shows the time evolution of the anomalies of zonal wind speed, $Z_{20°C}$, and surface zonal current along the equator from September 1997 to December 2010. The limits of the oligotophic region are indicated by the black contour in each panel. Anomalies of the surface current are superimposed on the surface chlorophyll anomalies during the peak period (September-February) of the 1997-1998 EP El Niño (Fig. 6) and 2002-2003 CP El Niño (Fig. 7).

5.1. The 1997-1998 EP El Niño event

During boreal fall of 1997, strong anomalous eastward currents dominate the equatorial Pacific (Fig. 5c; Fig. 6a-d) as a consequence of anomalous westerly winds (Fig. 5a) and forced downwelling Kelvin waves [Delcroix et al., 2000]. The South Equatorial Current (SEC) is weak or reversed and the NECC is stronger and shifted southwards [Johnson et al.,

2000]. As a result, nutrient-poor warm pool waters are advected eastward and reach 130°W during the mature phase in November 1997-January 1998 [Radenac et al., 2001]. The core of high negative chlorophyll anomaly is in the eastern part of the warm pool (Fig. 2c, 4b) where eastward surface currents are strong (Fig. 5c). Meanwhile, vertical supplies of nitrate and iron decrease or cease because of the reduction of the upwelling and the deepening of the nitracline and EUC [Fig. 5b; Chavez et al., 1999; Strutton and Chavez, 2000; Wilson and Adamec, 2001; Radenac et al., 2001; 2005]. A combination of these processes lead to a dramatic decrease of the surface chlorophyll and of the biological production in the central and eastern basins. The northern and southern limits of the negative chlorophyll anomaly closely match the extent of the eastward surface current anomaly until the peak period in December 1997 (Fig. 6a-d). Starting in January 1998, the surface chlorophyll anomaly weakens as strong westward surface currents begin to develop (Fig. 6d-e).

In the warm pool, the overall chlorophyll increase (Fig. 6a-f) has been ascribed to the thermocline rise (Fig. 5b) allowing nutrient input toward the lighted layer [Wilson and Adamec, 2001; Radenac et al., 2001; Turk et al., 2001]. Part of it, between 5°N and 10°N, results from enhanced chlorophyll concentration in the meanders of the nascent NECC observed seasonally between January and June and that were strong at the end of the 1997-1998 El Niño [Christian et al., 2004; Messié and Radenac, 2006]. Upwelling that develops along the coast of Papua New Guinea and Solomon Islands during favorable periods of westerly wind [Webster and Lukas, 1992; Kuroda, 2000; Ueki et al., 2003] also contributes to the chlorophyll increase in the warm pool south of the equator [Messié, 2006; Radenac et al., 2010].

5.2. The CP El Niño events

394 During CP El Niño events, the eastward shift of the warm pool (see the black contours in
395 figure 5a) in response to westerly winds is of lesser magnitude than during EP El Niño. The
396 associated equatorial eastward surface currents contribute to the development of negative
397 chlorophyll anomaly as a consequence of the penetration of the oligotrophic waters of the
398 warm pool toward the mesotrophic waters of the upwelling (Fig. 5c). The core of high
399 chlorophyll anomaly remains within the zone of quasi-persistent oligotrophic waters enclosed
400 by the 0.1 mg m^{-3} surface chlorophyll isoline in the eastern part of the warm pool (Fig. 2c),
401 near the zone of convergence between the eastward surface current in the warm pool and the
402 westward SEC east of it (Fig. 5c). The importance of this current convergence has been raised
403 by Kug et al. [2009] and Singh et al. [2011] to explain how SST and SSS anomaly cores could
404 remain confined in the central basin during CP El Niño.
405
406 During the 2002-2003 CP El Niño, the maximum negative chlorophyll anomaly is situated
407 around 170°E in June, 180°E in August, and it stays at 170°W between September and
408 December 2002 (Fig. 2c, 7a-d). It starts to move back to the west in January 2003 when
409 strong westward anomalies develop. The monthly maps of surface chlorophyll and current
410 (Fig. 7a-c) also suggest that anomalous eastward currents partly contribute to the equatorial
411 chlorophyll decrease towards the American coast.
412
413 As discussed above for CP El Nino, negative anomalies (weaker than -0.015 mg m^{-3}) are
414 constrained within 2° of the equator east of the high chlorophyll anomaly core (Fig. 4f). The
415 zonal wind anomaly is slightly westward in the eastern basin during the CP El Niño years
416 (Fig. 5a) and so cannot be responsible for a collapse of the upwelling in this region. Besides,
417 variations of the vertical supply of nitrate, depending on the nutrient pool depth represented
418 by the 20°C isotherm depth ($Z_{20°C}$), will not impact the phytoplankton growth as nitrate is

usually in excess in this region. The equatorial chlorophyll decrease would rather be the result of vertical displacements of the EUC that contribute modulating vertical iron fluxes and the phytoplankton growth in the iron limited ecosystem of the central and eastern equatorial Pacific. The temporal variability of the $Z_{20°C}$ anomaly can be used as an indicator of the EUC depth (Z_{EUC}) anomaly (Izumo, 2005). When ADCP currents are available at the equatorial mooring sites, the bias between Z_{EUC} (calculated as the depth of the maximum eastward velocity) and $Z_{20°C}$ is lower than 4 m at 170°W and 140°W and the correlation coefficient is 0.72 at both sites. Therefore, the variations of $Z_{20°C}$ reliably represent the variations of Z_{EUC} that deepens by 20-40 m during CP El Niño (Fig. 5b) and could drive a significant decrease of the vertical iron flux [Chavez et al., 1999]. A strip of maximum anomaly confined to the equator is consistent with the structure of meridional velocity and a narrow band of strong divergence roughly centered along the equator [Poulain, 1993]. This further suggests that biology along the equator is sensitive to the EUC depth and iron concentration.

Off the equator, the narrow zonal band of negative chlorophyll anomaly between 5°N and 10°N is observed during the four CP El Niño events. During the 2002-2003 CP El Niño event, it appears during August-September (Fig. 7a) and starts to break up during January-February (Fig. 7e). The negative chlorophyll anomaly strip follows the position of the eastward surface current anomaly (Fig. 7a-d), suggesting that nutrient- and phytoplankton-poor water from the warm pool is advected eastward by the strong NECC. Messié and Radenac [2006] showed the significant impact of the NECC variations on the surface chlorophyll seasonal variability in the western Pacific. During El Niño events, it is a basin-wide feature that participates in setting up the sharp chlorophyll front at the northern edge of the upwelling. In monthly chlorophyll maps, it is seen as a narrow band of oligotrohic waters extending from the warm pool to the Central American coast during October-December of all El Niño years (not

444 shown). South of the equator, negative chlorophyll anomalies coincide with a region of
445 southeastward surface currents that transport nutrient- and phytoplankton-poor waters toward
446 the Marquesas Islands (Fig. 7a-f). This feature is observed during September-February 2002-
447 2003, 2004-2005, and 2006-2007. It develops later during February-April during the 2009-
448 2010 CP El Niño event (not shown).
449
450 **6. Summary and discussion**
451 Enhanced attention has been given to global climate changes related to differences in the
452 location of SST anomalous warming in the tropical Pacific in recent years [Trenberth and
453 Stepaniak, 2001; Ashok et al., 2007; Kug et al., 2009; Kao and Yu, 2009; Yeh et al., 2009;
454 Lee and McPhaden, 2010]. To our knowledge, no attempt has been made so far to contrast the
455 biological conditions featuring the EP and CP El Niño, except for the recent study by Turk et
456 al. [2011]. To fulfill this gap, the goal of our study was to contrast and tentatively explain the
457 signature in chlorophyll of the EP and CP ENSO, for the 1997-2010 period.
458
459 During the SeaWiFS years, an AHC analysis of the surface chlorophyll anomaly shows that
460 EP El Niño occurred in 1997-1998, CP El Niño in 2002-2003, 2004-2005, 2006-2007, and
461 2009-2010, while La Niña lasted from 1998 to 2001 and from 2007 to 2009, consistent with
462 previous studies based on SST and SSS analyses (Table 1). Both types of El Niño events are
463 associated with an overall decrease of surface chlorophyll in the 10°S-10°N region. Yet,
464 spatial patterns differ between events.
465
466 During the 1997-1998 EP El Niño event, negative anomalies occupy most of the equatorial
467 basin between 10°S and 10°N, except for a chlorophyll increase in the western basin. A strong

468 negative chlorophyll anomaly (< -0.075 mg m^{-3}) is located at the equator between the date
469 line and 150°W and the oligotrophic warm pool is displaced eastward and reaches 130°W.
470
471 During the CP El Niño events, the equatorial anomaly is weaker (< -0.045 mg m^{-3}), shifted
472 westwards by about 20° of longitude, and the eastern edge of the oligotrophic warm pool is
473 confined west of 160°W. So, as already found for SST and SSS [Kug et al., 2009; Singh et al.,
474 2011], the region of strong chlorophyll anomaly is clearly shifted westward during CP El
475 Niño relative to EP El Niño. The location of these strong negative anomalies in the eastern
476 part of the warm pool suggests that oligotrophic waters of the warm pool replace mesotrophic
477 waters of the upwelling in the central basin, and that zonal advection is a major process
478 responsible for this signature. During CP El Niño, westward surface currents in the eastern
479 and central basins probably limit the eastward spreading of the negative chlorophyll anomaly
480 core.
481
482 Other mechanisms affecting nutrient or light availability could also lead to a chlorophyll
483 decrease in the central equatorial basin. One of them is the depth of the nutrient pool. The
484 core of high chlorophyll anomaly matches the maximum sea level anomaly [Kug et al., 2009;
485 Bosc et al., 2009] which reflects a strong depression of the thermocline [Rébert et al., 1985],
486 closely related to the depth of the nitracline in the oligotrophic warm pool. Besides, barrier
487 layer tends to be thick in the eastern edge of the warm pool [Maes et al., 2004; Bosc et al.,
488 2009] and to further isolate the deep nutrient pool from the lighted surface layer [Mackey et
489 al., 1995; Eldin et al., 1997; Murtugudde et al., 1999; Turk et al., 2001]. The nutrient pool is
490 deep on average in the oligotrophic warm pool and the depression of the nitracline in the
491 eastern part of the warm pool is probably a second order factor on surface chlorophyll
492 changes compared to the impact of advection.

493

494 Another factor accounting for chlorophyll changes during EP and CP El Niño could be the
495 reduction of incident light in the central Pacific as suggested by Park et al. [2011]. Zonal
496 extension of oligotrophic conditions is linked to the zonal extension of the warm pool, which
497 is the site of convective activity and moves eastward during El Niño. The average monthly
498 value of the satellite derived Photosynthetically Available Radiation (PAR) is 44.7 ±
499 4.4 Einstein m^{-2} d^{-1} in the eastern part of the warm pool while it is 48.6 ±2.2 Einstein m^{-2} d^{-1}
500 in the upwelling region at 140°W. The eastward shift of the convection zone leads to PAR
501 anomaly around 10 Einstein m^{-2} d^{-1} in the strong chlorophyll anomaly region in 1997-1998
502 and close to or less than 5 Einstein m^{-2} d^{-1} during the following El Niño events. These
503 relatively weak PAR variations, three to ten times weaker than variations at mid and high
504 latitudes [Letelier et al., 2004; Goes et al., 2004], suggest a weak impact on the phytoplankton
505 growth. Therefore, zonal advection and the resulting change of ecosystem in the central
506 Pacific are probably the dominant mechanisms responsible for the strong chlorophyll
507 anomaly, as also proposed by Messié and Chavez [submitted to J. Geophys. Res., 2012].
508 Mesotrophic waters of the upwelling with surface chlorophyll concentration around
509 0.2 mg m^{-3} are replaced by oligotrophic waters of the eastern part of the warm pool with
510 surface chlorophyll concentration lower than 0.07 mg m^{-3} [Radenac et al., 2010]. However,
511 separating the impact of the ecosystem change and of the light attenuation is not simple as
512 oligotrophic waters move simultaneously to the convection zone, and a process study is
513 needed to estimate each influence.
514

515 We suggest that the chlorophyll decrease along the equator east of the strong central Pacific
516 anomaly is the consequence of reduced vertical iron fluxes linked to the deepening of the
517 EUC during El Niño [Barber et al., 1996; Chavez et al., 1999; Wilson and Adamec, 2001;

518 Friedrichs and Hofmann, 2001]. Changes in the iron content of the EUC could also impact
519 biology in the central and eastern Pacific. Ryan et al. [2006] hypothesized that the
520 strengthening of the New Guinea Coastal Undercurrent (NGCUC), flowing northwestward
521 along the northern coast of Papua New Guinea, favored transport of iron from shelf sediments
522 that feeds the EUC during El Niño years, which in turn favored phytoplankton blooms
523 observed in the central Pacific following El Niño events. In contrast, setting the iron
524 concentration proportional to the NGCUC speed in the source region did not change the
525 intensity of eastern equatorial Pacific blooms in a simulation based study [Gorgues et al.,
526 2010]. Thus, although the impact of a continental iron source in the western equatorial Pacific
527 on the biogeochemistry of the equatorial upwelling region has been shown in several
528 modeling studies [Christian et al., 2002; Vichi et al., 2008; Slemons et al., 2009; Gorgues et
529 al., 2010], the influence of a variable iron supply into the EUC on the ecosystems of the
530 central and eastern basins is still unclear. So is the role of tropical instability waves (TIW).
531 Because of vigorous horizontal processes as well as upwelling and downwelling, localized
532 maximum and minimum of phytoplankton biomass characterize TIW [Yoder et al., 1994;
533 Strutton et al., 2001; Menkes et al., 2002]. Their net impact on phytoplankton biomass has
534 been estimated to be positive [Barber et al., 1996; Friedrichs and Hofmann, 2001; Strutton et
535 al., 2001] or negative [Gorgues et al., 2005]. Other studies show an enhancement or decrease
536 of the phytoplankton biomass depending on interactions between the large scale
537 thermocline/ferricline depth and the intensity of the local TIW dynamics [Vichi et al., 2008;
538 Evans et al., 2009]. The reduction or absence of TIW activity during El Niño [Legeckis, 1977;
539 Friedrichs and Hofmann, 2001; Evans et al., 2009] can also possibly contribute to the
540 chlorophyll decrease observed along the equator.
541

The AHC analysis of the 1997-2010 surface chlorophyll anomaly dataset does not separate La Niña events into EP and CP events. Chlorophyll increases in the equatorial western basin and near 8-10°N and toward the Marquesas Islands are common patterns to La Niña maps. Nevertheless, the location of the equatorial core of positive anomalies and its magnitude change (much stronger in 2010 than during other events) and an equatorial increase in the central and eastern basins may not be observed. The average location of chlorophyll anomaly of the six La Niña events seen by SeaWiFS is situated west of the EP and CP El Niño anomalies. This is consistent with the La Niña signature as reported by Kug et al. [2009] and Kug and Ham [2011] who do not separate CP and EP cold events in terms of SST anomaly. Besides, the chlorophyll anomaly analysis does not evidence any symmetry between the warm and cold phases of ENSO events as suggested in Kao and Yu [2009] and Yu et al. [2010] analyses. The distinct EP and CP La Niña patterns mentioned by Singh et al. [2011] are based on a cluster analysis of SSS that captures a signal in the SPCZ region that does not show up in the chlorophyll analysis.

During La Niña years, the equatorial core of positive anomaly results from the westward expansion of the upwelling mesotrophic waters in a region where the usual surface chlorophyll concentration does not exceed 0.1 mg m^{-3} (Fig. 2c). The weak nutrient supply to the euphotic layer in the Niño4 region results from horizontal advection of nutrient-rich waters from the east and upward advection [Stoens et al., 1999]. During La Niña events, observational and modeling studies have shown that upwelling led to increased surface chlorophyll concentration in the western Pacific [Blanchot et al., 1992; Radenac and Rodier, 1996; Radenac et al., 2001]. East of the strong anomaly core, the iron limitation and the grazing pressure (small phytoplankton and zooplankton species dominate the ecosystem and microzooplankton can quickly respond to changes in nano- and pico-phytoplankton biomass)

567 control the ecosystem resulting in a monotonously low phytoplankton biomass in the
568 equatorial divergence [Chavez et al., 1991; Le Bouteiller and Blanchot, 1991; Strutton et al.,
569 2008]. This special feature of the equatorial upwelling ecosystem could explain why no strong
570 chlorophyll increase characterizes the overall La Niña distribution of chlorophyll anomaly
571 along the equator east of the anomaly core (Fig. 4d). An asymmetry between El Niño and La
572 Niña has also been observed in terms of temperature (Larkin and Harrison, 2002; An and Jin,
573 2004). The warm phase of ENSO is often stronger than its cold phase. Nonlinear dynamical
574 processes could impact nutrient (iron) supply and cause an asymmetry of the ENSO-related
575 biological response as they impact the ENSO-related heat budget (An and Jin, 2004). More
576 investigations remain to be done on this issue, especially during the CP El Niño events that
577 dominate during the recent years. Cluster 2 in the AHC analysis (Fig. 4a, c) captured
578 exceptions to this uniformity. 80% of the maps that compose this cluster come from the 1998
579 La Niña year when unusual large-scale blooms [Ryan et al., 2002] were observed in the
580 equatorial Pacific after the major 1997-1998 EP El Niño event. Chlorophyll increases
581 subsequent to island mass effect generated by the Kiribati Islands, which behave as an
582 obstacle to both the SEC and the EUC between February and June 1998 [Ryan et al., 2002;
583 Messié et al., 2006] may contribute to the positive anomaly observed west of the dateline. A
584 second bloom, the longest and more intense one with chlorophyll concentration higher than
585 0.8 mg m^{-3}, developed between 160°W and 140°W and then spread eastward from June to
586 September [Chavez et al., 1999; Ryan et al., 2002; Gorgues et al., 2010]. The last bloom was
587 observed around 130°W during November-December 1998 [Ryan et al., 2002]. Reasons for
588 these blooms can be both large-scale and local dynamics, such as, enhanced iron vertical
589 fluxes because of a shallower thermocline and more active TIW during La Niña. A similar but
590 somewhat weaker situation seemed to occur in mid-2010. Interestingly, these equatorial
591 recovery conditions occur when strong El Niño events turn swiftly into strong La Niña: from

592 the major 1997-1998 EP El Niño to the strong 1998-1999 La Niña [Chavez et al., 1999; Ryan
593 et al., 2002; Radenac et al., 2010] and from the strong 2009-2010 CP El Niño to the strong
594 2010-2011 La Niña [Kim et al., 2011]. These periods coincide with phases of reduced grazing
595 pressure as a response to El Niño related reduced phytoplankton biomass and productivity.
596 Therefore, momentarily low grazing pressure probably combines to dynamical impacts
597 leading to enhanced phytoplankton growth to drive high phytoplankton biomass during these
598 recovery periods after strong El Niño events [Strutton and Chavez, 2000; Friedrichs and
599 Hofmann, 2001; Gorgues et al., 2010].
600
601 While increased eastward advection was responsible for the chlorophyll decreases along 8-
602 10°N and towards the Marquesas Islands during CP El Niño, the chlorophyll increases at the
603 same locations during La Niña coincide with increased westward and poleward surface
604 currents suggesting the influence of horizontal advection.
605
606 Situations that occurred in 2001-2002, 2003-2004, 2005-2006, and 2007 close to CP El Niño
607 years (Figs. 4a, e) were called intermediate CP El Niño conditions. Their spatial structure
608 (Fig. 4e) is characterized by an anomaly core of about -0.04 mg m^{-3} located near 160°E. The
609 persistent negative chlorophyll anomaly in the western Pacific could be specific to the period
610 we study (recurring CP El Niño conditions) and this is why we do not refer to it as neutral
611 conditions.
612
613 The SeaWiFS archive spans over more than 13 years during which 5 El Niño events occur.
614 Interestingly, the AHC analysis we performed on the monthly surface chlorophyll anomaly
615 maps separates the 1997-1998 EP episode from the other CP El Niño episodes. These results
616 need to be refined with the help of longer observational time series, modeling outputs, and

theoretical work. An improve understanding of the phytoplankton distribution and its temporal variability is actually essential to anticipate biogeochemical climate-driven shifts and their consequences on ocean dynamics, carbon cycle, and marine ressources. Different phytoplankton distribution during CP and EP El Niño events could actually impact the distribution and abundance of exploited fish species such as tuna, whose fishery in the central and western tropical Pacific is one of the largest industrial fisheries of the world [Lehodey et al., 2011]. Complementing our qualitative analysis, we also need to quantify how physical and/or biological processes lead to the contrasted patterns we evidenced.

Acknowledgements

We acknowledge the SeaWiFS Project at GSFC (http://oceancolor.gsfc.nasa.gov), the Hadley Centre for Climate Prediction and Research Sea Ice and Sea Surface Temperature (http://www.metoffice.gov.uk/hadobs/hadisst), OSCAR (http://www.oscar.noaa.gov), the SSS Observation Service (http://www.legos.obs-mip.fr/observations/sss), and the TOGA-TAO Project Office of NOAA/PMEL (http://www.pmel.noaa.gov/tao) for sharing the freely available data we used. We also used time series of the Southern Oscillation Index (http://www.cpc.ncep.noaa.gov/data/indices/soi) and of the El Niño Modoki Index (http://www.jamstec.go.jp/frcgc/research/d1/iod/modoki_home.html.en). This work was supported by CNES in the frame of the Ocean Surface Topography Science Team program. F. L. benefited from CNES funding and A. S. benefits from a PhD grant from the Institut de Recherche pour le Développement (IRD). We thank the two reviewers for their useful comments.

References

641 An, S.-I. and F.-F. Jin (2004), Nonlinearity and asymmetry of ENSO. *J. Clim., 17*, 2399–
642 2412.
643 Ashok, K., S. K. Behera, S. A. Rao, H. Weng, and T .Yamagata (2007), El Niño Modoki and
644 its teleconnection, *J. Geophys. Res., 112*, C11007, doi:10.1029/2006JC003798.
645 Barber, R. T. and J. E. Kogelschatz (1990), Nutrients and productivity during the 1982/83 El
646 Niño. In: *Global ecological consequences of the 1982-83 El Niño-Southern oscillation*,
647 edited by P. W. Glynn, pp. 31-53, Elsevier, Amsterdam.
648 Barber, R. T., M. P. Sanderson, S. T. Lindley, F. Chai, J. Newton, C. C. Trees, D. G. Foley,
649 and F. P. Chavez (1996), Primary productivity and its regulation in the equatorial Pacific
650 during and following the 1991-1992 El Niño. *Deep-Sea Res. II, 43*, 933-969.
651 Blanchot, J., M. Rodier, and A. Le Bouteiller (1992), Effect of El Niño Southern Oscillation
652 events on the distribution and abundance of phytoplankton in the western Pacific Ocean
653 along 165°E. *J. Plankton Res., 4*, 137-156.
654 Bonjean, F. and G.S.E. Lagerloef (2002), Diagnostic model and analysis of the surface
655 currents in the tropical Pacific ocean. *J. Phys. Oceanogr., 32*, 2938-2954.
656 Bosc, C., T. Delcroix, and C. Maes (2009), Barrier layer variability in the western Pacific
657 warm pool from 2000 to 2007, *J. Geophys. Res., 114*, C06023,
658 doi:10.1029/2008JC005187.
659 Campbell, J. W., J. M. Blaisdell, and M. Darzi (1995), Level-3 SeaWiFS data products:
660 Spatial and temporal binning algorithms, *NASA Technical Memorandum, 32*, 104566, 80
661 pp.
662 Chavez, F. P., K. R. Buck, K. H. Coale, J. H. Martin, G. R. DiTullio, N. A. Welschmeyer, A.
663 C. Jacobson, and R. T. Barber (1991), Growth rates, grazing, sinking, and iron limitation
664 of equatorial Pacific phytoplankton. *Limnol. Oceanogr., 36*, 1816-1833.

665 Chavez, F. P., P. G. Strutton, and M. J. McPhaden (1998), Biological-physical coupling in the
666 central Pacific during the onset of the 1997-98 El Niño. *Geophys. Res. Lett., 25*, 3543-
667 3546.
668 Chavez, F. P., P. G. Strutton, G. E. Friederich, R. A. Feely, G. C. Feeldman, D. G. Foley, and
669 M. J. McPhaden (1999), Biological and chemical response of the equatorial Pacific Ocean
670 to the 1997-98 El Niño. *Science, 286*, 2126-2131.
671 Christian, J. R., M. A. Verschell, R. Murtugudde, A. J. Busalacchi, and C. R. McClain (2002),
672 Biogeochemical modelling of the tropical Pacific ocean. II. Iron biogeochemistry. *Deep-*
673 *Sea Res. II, 49*, 545-565.
674 Christian, J. R., R. Murtugudde, J. Ballabrera-Poy, and C. R. McClain (2004), A ribbon of
675 dark water: phytoplankton blooms in the meanders of the Pacific North Equatorial
676 Countercurrent. *Deep-Sea Res. II, 51*, 209-228.
677 Delcroix, T., B. Dewitte, Y. duPenhoat, F. Masia, and J. Picaut (2000), Equatorial waves and
678 warm pool displacements during the 1992-1998 El Niño Southern Oscillation events:
679 Observation and modeling. *J. Geophys. Res., 105*, 14357-14373.
680 Delcroix, T., G. Alory, S. Cravatte, T. Corrège, and M. J. McPhaden (2011), A gridded sea
681 surface salinity data set for the tropical Pacific with sample applications (1950–2008).
682 *Deep-Sea Res. I, 58*, 38-48.
683 Eldin, G., M. Rodier, and M. H. Radenac (1997), Physical and nutrient variability in the upper
684 equatorial Pacific associated with westerly wind forcing and wave activity in October
685 1994. *Deep-Sea Res. II, 44*, 1783-1800.
686 Evans, W., P. G. Strutton, and F. P. Chavez (2009), Impact of tropical instability waves on
687 nutrient and chlorophyll distributions in the equatorial Pacific. *Deep-Sea Res. I, 56*, 178-
688 188.

689 Friedrichs, M. A. M. and E. E. Hofmann (2001), Physical control of biological processes in
690 the central equatorial Pacific Ocean. *Deep-Sea Res. I, 48*, 1023-1069.
691 Frouin, R., B. A. Franz and P. J. Werdell (2003), The SeaWiFS PAR product. In *Algorithm*
692 *Updates for the Fourth SeaWiFS Data Reprocessing*, edited by S. B. Hooker and E. R.
693 Firestone, pp. 46–50, NASA/TM-2003-206892, 22.
694 Glantz, M. H. (2000), *Currents of Change: Impacts of El Niño and La Niña on climate and*
695 *society*. Cambridge, UK: Cambridge University Press. 266 pp.
696 Goes, J. I., K. Sasaoka, H. Do R. Gomes, S.-I. Saitoh, and T. Saino (2004), A comparison of
697 the seasonality and interannual variability of phytoplankton biomass and production in the
698 western and eastern gyres of the subarctic Pacific using multi-sensor satellite data. *J.*
699 *Oceanogr., 60*, 75-91.
700 Gordon, R. M., K. H. Coale, and K. S. Johnson (1997), Iron distribution in the equatorial
701 Pacific: Implications for new production. *Limnol. Oceanogr., 43*, 419-431.
702 Gorgues, T., C. Menkes, O. Aumont, J. Vialard, Y. Dandonneau, and L. Bopp (2005),
703 Biogeochemical impact of tropical instability waves in the equatorial Pacific. *Geophys.*
704 *Res. Lett., 32*, L24615, doi:10.1029/2005GL024110.
705 Gorgues, T., C. Menkes, L. Slemons, O. Aumont, Y. Dandonneau, M.-H. Radenac, S. Alvain,
706 and C. Moulin (2010), Revisiting the La Niña 1998 phytoplankton blooms in the
707 equatorial Pacific. *Deep-Sea Res. I, 57*, 567-576.
708 Hsieh W. W. (2001) Nonlinear canonical correlation analysis of the tropical Pacific climate
709 variability using a neural network approach. *J. Clim., 14*, 2528–2539.
710 Izumo, T. (2005), The equatorial undercurrent, meridional overturning circulation, and their
711 roles in mass and heat exchanges during El Niño events in the tropical Pacific ocean.
712 *Ocean Dyn., 55*, 110-123.

713 Johnson, G. C., M. J. McPhaden, G. D. Rowe, and K. E. McTaggart (2000), Upper equatorial
714 Pacific ocean current and salinity variability during the 1996-1998 El Niño-La Niña cycle.
715 *J. Geophys. Res., 105*, 1037-1053.
716 Kao, H.-Y. and J.-Y. Yu (2009), Contrasting eastern-Pacific and central-Pacific types of
717 ENSO. *J. Clim., 22*, 615-632.
718 Kim, H.-M., P. J. Webster, and J. A. Curry (2009), Impact of shifting patterns of Pacific
719 ocean warming on north Atlantic tropical cyclones. *Science, 325*, 5936, 77-80.
720 Kim, W., S.-W. Yeh, J.-H. Kim, J.-S. Kug, and M. Kwon (2011), The unique 2009–2010 El
721 Niño event: A fast phase transition of warm pool El Niño to La Niña, *Geophys. Res. Lett.*,
722 38, L15809, doi:10.1029/2011GL048521.
723 Kug, J.-S., and Y.-G. Ham (2011), Are there two types of La Nina?, *Geophys. Res. Lett., 38*,
724 L16704, doi:10.1029/2011GL048237.
725 Kug, J.-S., F.-F. Jin, and S.-I. An (2009), Two types of El Niño events: cold tongue El Niño
726 and warm pool El Niño. *J. Clim., 22*, 1499–1515, doi: 10.1175/2008JCLI2624.1.
727 Kuroda, Y. (2000), Variability of currents off the northern coast of New Guinea. *J.*
728 *Oceanogr., 56*, 103-116.
729 Lacan, F. and C. Jeandel (2001), Tracing Papua New Guinea imprint on the central Equatorial
730 Pacific Ocean using neodymium isotopic compositions and Rare Earth Element patterns.
731 *Earth Planet. Sci. Lett., 186*, 497-512.
732 Landry, M. R., R. T. Barber, R. R. Bidigare, F. Chai, K. H. Coale, H. G. Dam, M. R. Lewis,
733 S. T. Lindley, J. J. McCarthy, M. R. Roman, D. K. Stoecker, P. G. Verity, and J. R. White
734 (1997), Iron and grazing constraints on primary production in the central equatorial
735 Pacific: An EqPac synthesis. *Limnol. Oceanogr., 42*, 405-418.

736 Larkin, N. K. and D. E. Harrison (2002), ENSO warm (El Niño) and cold (La Niña) event life
737 cycles: ocean surface anomaly patterns, their symmetries, asymmetries, and implications.
738 *J. Clim., 15*, 1118-1140.
739 Le Borgne, R., R. T. Barber, T. Delcroix, H. Y. Inoue, D. J. Mackey, and M. Rodier (2002),
740 Pacific warm pool and divergence: temporal and zonal variations on the equator and their
741 effects on the biological pump. *Deep-Sea Res. II, 49*, 2471-2512.
742 Le Bouteiller, A. and J. Blanchot (1991), Size distribution and abundance of phytoplankton in
743 the Pacific equatorial upwelling, *La Mer, 29*, 175-179.
744 Lee, T. and M. J. McPhaden (2010), Increasing intensity of El Niño in the central-equatorial
745 Pacific, *Geophys. Res. Lett., 37*, L14603, doi:10.1029/2010GL044007.
746 Legeckis, R. (1977), Long waves in the eastern equatorial Pacific Ocean: A view from a
747 geostationary satellite. *Science, 197*, 1179-1181.
748 Lehodey, P., J. Hampton, R. W. Brill, S. Nicol, I. Senina, B. Calmettes, H. O. Pörtner, L.
749 Bopp, T. Ilyina, J. D. Bell, and J. Sibert (2011), Vulnerability of oceanic fisheries in the
750 tropical Pacific to climate change. In: *Vulnerability of Tropical Pacific Fisheries and*
751 *Aquaculture to Climate Change*. Edited by J. D. Bell, J. E. Johnson and A. J. Hobday, pp.
752 433-492, Secretariat of the Pacific Community, Noumea, New Caledonia.
753 Leloup, J., M. Lengaigne, and J.-P. Boulanger (2007), Twentieth century ENSO
754 characteristics in the IPCC database. *Clim. Dyn., 30*, 277-291.
755 Letelier, R. M., D. M. Karl, M. R. Abbott and R. R. Bidigare (2004), Light driven seasonal
756 patterns of chlorophyll and nitrate in the lower euphotic zone of the north pacific
757 subtropical gyre. *Limnol. Oceanogr., 49*, 508-519.
758 Mackey, D. J., J. Parslow, H. W. Higgins, F. B. Griffiths, and J. E. O'Sullivan (1995),
759 Plankton productivity and biomass in the western equatorial Pacific: biological and
760 physical controls. *Deep-Sea Res. II, 42*, 499-533.

761 Maes, C., J. Picaut, Y. Kuroda, and K. Ando (2004), Characteristics of the convergence zone
762 at the eastern edge of the Pacific warm pool. *Geophys. Res. Lett., 31*, L11304, doi:
763 10.1029/2004GL019867.
764 McClain, C. R., G. C. Feldman, and S. B. Hooker (2004), An overview of the SeaWiFS
765 project and strategies for producing a climate research quality global ocean bio-optical
766 time series. *Deep-Sea Res. II, 51*, 5-42.
767 McPhaden, M. J., A. J. Busalacchi, R. Cheney, J.-R. Donguy, K. S. Gage, D. Halpern, M. Ji,
768 P. Julian, G. Meyers, G. T. Mitchum, P. P. Niiler, J. Picaut, R. W. Reynolds, N. Smith,
769 and K. Takeuchi (1998), The Tropical Ocean-Global Atmosphere observing system: A
770 decade of progress. *J. Geophys. Res., 103*, 14169-14240.
771 McPhaden, M. J., S. E. Zebiak, and M. H. Glantz (2006), ENSO as an integrating concept in
772 Earth science, *Science, 314*, 5806, 1740-1745, doi:10.1126/science.1132588.
773 McPhaden, M. J., T. Lee, and D. McClurg (2011), El Niño and its relationship to changing
774 background conditions in the tropical Pacific Ocean, *Geophys. Res. Lett., 38*, L15709,
775 doi:10.1029/2011GL048275.
776 Menkes, C., S. C. Kennan, P. Flament, Y. Dandonneau, S. Masson, B. Biessy, E. Marchal, G.
777 Eldin, J. Grelet, Y. Montel, A. Morliere, A. Lebourges-Dhaussy, C. Moulin, G.
778 Champalbert and, A. Herbland (2002), A whirling ecosystem in the Equatorial Atlantic,
779 *Geophys. Res. Lett., 11*, 1553, doi: 10.1029/2001GL014576.
780 Messié, M. (2006), Contrôle de la dynamique de la biomasse phytoplanctonique dans le
781 Pacifique tropical ouest. Thèse de doctorat de l'Univ. Toulouse 3, France, 263 pp.
782 Messié, M. and M.-H. Radenac (2006), Seasonal variability of the surface chlorophyll in the
783 western tropical Pacific from SeaWiFS data. *Deep-Sea Res. I, 53*, 10, 1581-1600.

784 Messié, M., M.-H. Radenac, J. Lefèvre, and P. Marchesiello (2006), Chlorophyll bloom in the
785 western Pacific at the end of the 1997-98 El Niño: the role of Kiribati Islands, *Geophys.*
786 *Res. Lett., 33*, L14601, doi:10.1029/2006GL026033.
787 Murtuggude, R. G., S. R. Signorini, J. R. Christian, A. J. Busalacchi, C. R. McClain, and J.
788 Picaut (1999), Ocean color variability of the tropical Indo-Pacific basin observed by
789 SeaWiFS during 1997-98. *J. Geophys. Res., 104*, 18351-18365.
790 Park, J.-Y., J.-S. Kug, J.-S. Park, S.-W. Yeh, and C. J. Jang (2011), Variability of chlorophyll
791 associated with ENSO and its possible biological feedback in the Equatorial Pacific, *J.*
792 *Geophys. Res.*, doi:10.1029/2011JC007056.
793 Picaut, J. and T. Delcroix (1995), Equatorial wave sequence associated with warm pool
794 displacement during the 1986-1989 El Niño-La Niña. *J. Geophys. Res., 100*, 18393-
795 18408.
796 Picaut, J., M. Ioualalen, T. Delcroix, F. Masia, R. Murtugudde, and J. Vialard (2001), The
797 oceanic zone of convergence on the eastern edge of the Pacific warm pool: A synthesis of
798 results and implications for El Niño-Southern Oscillation and biogeochemical phenomena.
799 *J. Geophys. Res., 106*, 2363-2386.
800 Poulain, P.-M. (1993), Estimates of horizontal divergence and vertical velocity in the
801 equatorial Pacific. *J. Phys. Oceanogr., 23*, 601-607.
802 Radenac, M.-H. and M. Rodier (1996), Nitrate and chlorophyll distributions in relation to
803 thermohaline and current structures in the western tropical Pacific during 1985-1989.
804 *Deep-Sea Res. II, 43*, 725-752.
805 Radenac, M.-H., C. Menkes, J. Vialard, C. Moulin, Y. Dandonneau, T. Delcroix, C. Dupouy,
806 A. Stoens, and P.-Y. Deschamps (2001), Modeled and observed impacts of the 1997-1998
807 El Niño on nitrate and new production in the equatorial Pacific, *J. Geophys. Res., 106*,
808 26879-26898.

809 Radenac, M.-H., Y. Dandonneau, and B. Blanke (2005), Displacements and transformations
810 of nitrate-rich and nitrate-poor water masses in the tropical Pacific during the 1997 El
811 Niño, *Ocean Dyn., 55*, 34-46, DOI: 10.1007/s10236-005-0111-5.
812 Radenac, M.-H., P. E. Plimpton, A. Lebourges-Dhaussy, L. Commien, and M. J. McPhaden
813 (2010), Impact of environmental forcing on the acoustic backscattering strength in the
814 equatorial Pacific: diurnal, lunar, intraseasonal, and interannual variability, *Deep-Sea Res.*
815 *I, 57*, 1314-1328.
816 Rasmusson, E. M. and T. H. Carpenter (1982), Variations in tropical sea surface temperature
817 and surface wind fields associated with the Southern Oscillation/El Niño. *Mon. Weather*
818 *Rev., 110*, 354–384.
819 Rayner, N. A., D. E. Parker, E. B. Horton, C. K. Folland, L. V. Alexander, D. P. Rowell, E. C.
820 Kent, and A. Kaplan (2003), Global analyses of sea surface temperature, sea ice, and night
821 marine air temperature since the late nineteenth century, *J. Geophys. Res., 108*, 4407,
822 doi:10.1029/2002JD002670.
823 Rébert, J.-P., J.-R. Donguy, G. Eldin, and K. Wyrtki (1985), Relations between sea-level,
824 thermocline depth, heat content, and dynamic height in the tropical Pacific. *J. Geophys.*
825 *Res., 90*, 11719-11725.
826 Ren, H.-L. and F.-F. Jin (2011), Niño indices for two types of ENSO, *Geophys. Res. Lett., 38*,
827 L04704, doi:10.1029/2010GL046031.
828 Ryan, J. P., P. S. Polito, P. G. Strutton, and F. P. Chavez (2002), Unusual large-scale
829 phytoplankton blooms in the equatorial Pacific. *Prog. Oceanogr., 55*, 263-285.
830 Ryan, J. P., I. Ueki, Y. Chao, H. Zhang, P. S. Polito, and F. P. Chavez (2006), Western Pacific
831 modulation of large phytoplankton blooms in the central and eastern equatorial Pacific. *J.*
832 *Geophys. Res., 111*, G02013, doi: 10.1029/2005JG000084.

833 Singh, A., T. Delcroix, and S. Cravatte (2011), Contrasting the flavors of El Niño-Southern
834 Oscillation using sea surface salinity observations. *J. Geophys. Res., 116*, C06016,
835 doi:10.1029/2010JC006862.
836 Singh, A., and T. Delcroix (2011), Estimating the effects of ENSO upon the observed
837 freshening trends of the western tropical Pacific Ocean. *Geophys. Res. Lett., 38*, L21607,
838 doi:10.1029/2011GL049636.
839 Slemons, L. O., J. W. Murray, J. Resing, B. Paul, and P. Dutrieux (2010), Western Pacific
840 coastal sources of iron, manganese, and aluminum to the Equatorial Undercurrent, *Global*
841 *Biogeochem. Cycles, 24*, GB3024, doi:10.1029/2009GB003693.
842 Stoens, A., C. Menkes, M.-H. Radenac, N. Grima, Y. Dandonneau, G. Eldin, L. Memery, C.
843 Navarette, J.-M. André, T. Moutin, and P. Raimbault (1999), The coupled physical-new
844 production system in the equatorial Pacific during the 1992-1995 El Niño. *J. Geophys.*
845 *Res., 104*, 3323-3339.
846 Strutton, P. G. and F. P. Chavez (2000), Primary productivity in the equatorial Pacific during
847 the 1997-98 El Niño. *J. Geophys. Res., 105*, 26089-26101.
848 Strutton, P. G., J. P.Ryan, and F. P.Chavez (2001), Enhanced chlorophyll associated with
849 tropical instability waves in the equatorial Pacific. *Geophys. Res. Lett., 28*, 2005-2008.
850 Strutton, P. G., W. Evans, and F. P. Chavez (2008), Equatorial Pacific chemical and
851 biological variability, 1997-2003. *Global Biogeochem. Cycles,* 22, GB2001,
852 doi:10.1029/2007GB003045.
853 Takahashi, K., A. Montecinos, K. Goubanova, and B. Dewitte (2011), ENSO regimes:
854 Reinterpreting the canonical and Modoki El Niño, *Geophys. Res. Lett., 38*, L10704,
855 doi:10.1029/2011GL047364.
856 Trenberth, K. E. and D. P. Stepaniak (2001), Indices of El Niño evolution. *J. Clim., 14*, 1697-
857 1701.

858 Turk, D., M. R. Lewis, G. W. Harrison, T. Kawano, and I. Asanuma (2001), Geographical
859 distribution of new production in the western/central equatorial Pacific during El Niño and
860 non-El Niño conditions. *J. Geophys. Res., 106*, 4501-4515.
861 Turk, D., C. S. Meinen, D. Antoine, M. J. McPhaden, and M. R. Lewis (2011), Implications
862 of changing El Niño patterns for biological dynamics in the equatorial Pacific Ocean.
863 *Geophys. Res. Lett.*, doi:10.1029/2011GL049674, in press.
864 Ueki, I., Y. Kashino, and Y. Kuroda (2003), Observation of current variations off the New
865 Guinea coast including the 1997-1998 El Niño period and their relationship with Sverdrup
866 transport. *J. Geophys. Res., 108*, 3243, doi:10.1029/2002JC001611.
867 Vialard, J., C. Menkes, J.-P. Boulanger, P. Delecluse, E. Guilyardi, M. J. McPhaden, and G.
868 Madec (2001), A model study of oceanic mechanisms affecting equatorial Pacific sea
869 surface temperature during the 1997-98 El Niño. J.*Phys. Oceanogr., 31*, 1649-1675.
870 Vichi, M., S. Masina, and F. Nencioli (2008), A process-oriented model study of equatorial
871 Pacific phytoplankton: The role of iron supply and tropical instability waves. *Prog.*
872 *Oceanogr., 78*, 147-162.
873 Vincent, E. M., M. Lengaigne, C. E. Menkes, N. C. Jourdain, P. Marchesiello and G. Madec
874 (2009), Interannual variability of the South Pacific Convergence Zone and implications
875 for tropical cyclone genesis. *Clim. Dyn*., DOI 10.1007/s00382-009-0716-3.
876 Webster, P. J. and R. Lukas (1992), TOGA-COARE: the Coupled Ocean-Atmosphere
877 Response Experiment. *Bull. Am. Meteorol. Soc., 73*, 1377-1416.
878 Wells, M. L., G. K. Vallis, and E. A. Silver (1999), Tectonic processes in Papua New Guinea
879 and past productivity in the eastern equatorial Pacific Ocean. *Nature, 398*, 6728, 601-604.
880 Wilson, C. and D. Adamec (2001), Correlations between surface chlorophyll and sea surface
881 height in the tropical Pacific during the 1997-1999 El Niño-Southern Oscillation event. *J.*
882 *Geophys. Res., 106*, 31175-31188.

883 Yeh, S.-W., J.-S. Kug, B. Dewitte, M.-H. Kwon, B. P. Kirtman, and F.-F. Jin (2009), El Niño
884 in a changing climate. *Nature, 416*, 511-514.
885 Yoder, J. A. and M. Kennelly (2003), Seasonal and ENSO variability in global ocean
886 phytoplankton chlorophyll derived from 4 years of SeaWiFS measurements. *Global*
887 *Biogeochem. Cycles, 17*, 1112, doi: 10.1029/2002GB001942.
888 Yoder, J. A., S. G. Ackleson, R. T. Barber, P. Flament and W. M. Balch (1994), A line in the
889 sea. *Nature, 371*, 689– 692.
890 Yu, J.-Y. and S. T. Kim (2010), Identification of Central-Pacific and Eastern-Pacific types of
891 ENSO in CMIP3 models, *Geophys. Res. Lett., 37*, L15705, doi:10.1029/2010GL044082.
892 Yu, J.-Y., H.-Y. Kao, T. Lee, and S. T. Kim (2010), Subsurface ocean temperature indices for
893 central-Pacific and eastern-Pacific types of El Nino and La Nina events. *Theor. Appl.*
894 *Climatol.*, DOI: 10.1007/s00704-010-0307-6.
895

Table 1. Classification of ENSO events as Central Pacific (CP) or Eastern Pacific (EP) El Niño (EN) or La Niña (LN). All studies used SST except (1) used SSS and (2) used chlorophyll to characterize ENSO.

	97-98	98-99	99-00	00-01	02-03	04-05	05-06	06-07	07-08	08-09	09-10	10
Ashok et al. [2007]					CP EN	CP EN						
Kim et al. [2009]	EP EN	EP LN	EP LN		CP EN	CP EN						
Yeh et al. [2009]	EP EN				CP EN	CP EN		EP EN				
Kao and Yu [2009]	EP EN	CP LN	CP LN		CP EN	CP EN	EP LN					
Kug et al. [2009]	EP EN	LN	LN	LN	CP EN	CP EN	LN					
Lee and McPhaden [2010]	EP EN	LN			CP EN	CP EN		EP EN	LN		CP EN	
Ren and Jin [2011]	EP EN	LN	LN		CP EN	CP EN		CP EN	LN		CP EN	
[(1)]Singh et al. [2011]	EP EN	CP LN	EP LN	EP LN	CP EN	CP EN	EP LN	CP EN	EP LN	EP LN		
McPhaden et al. [2011]	EP EN				CP EN	CP EN		EP EN			CP EN	
[(2)]This study	EP EN	LN	LN	LN	CP EN	CP EN		CP EN	LN	LN	CP EN	LN

899

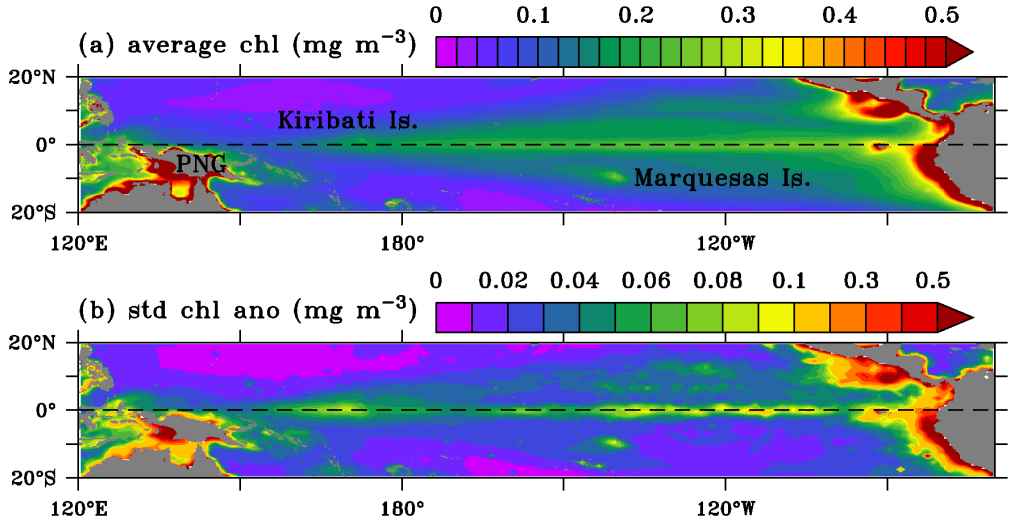

1 **Figure 1**. Maps of (a) average and (b) interannual standard deviation of the surface

2 chlorophyll computed over the September 1997 - December 2010 period. PNG stands for

3 Papua New Guinea.

4

5

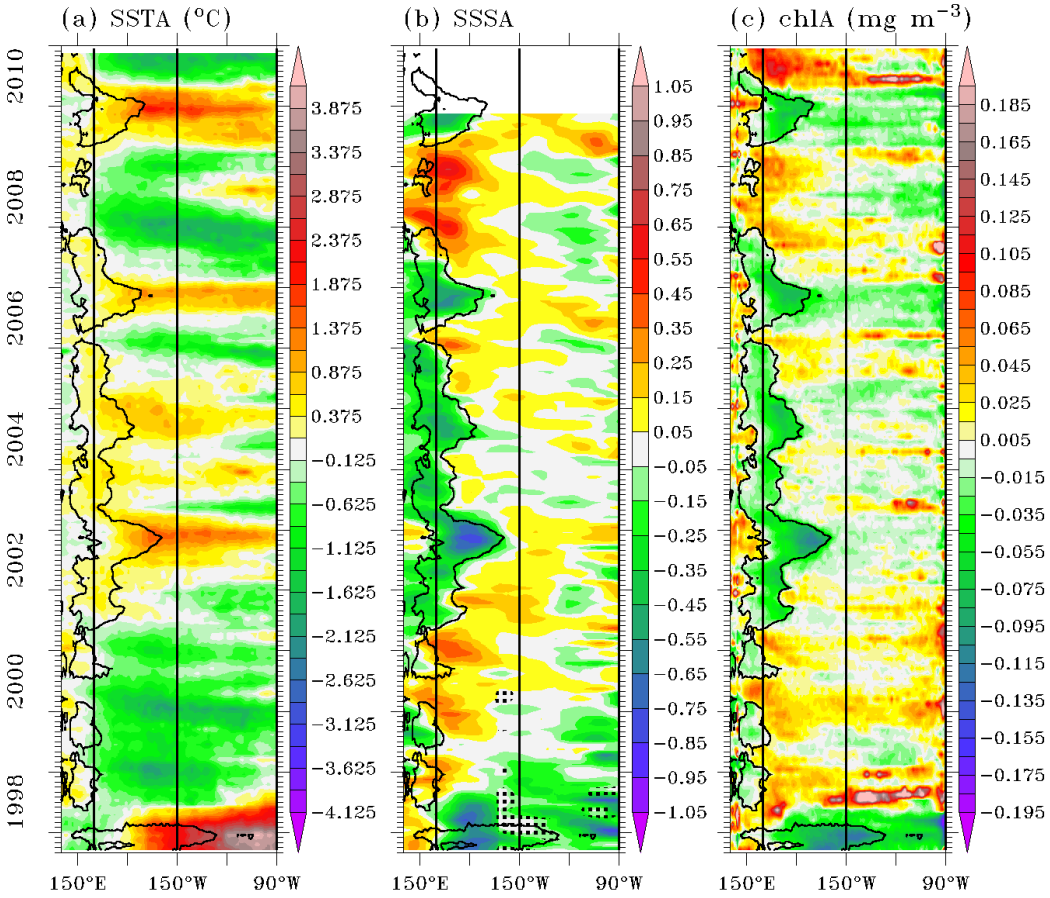

Figure 2. Longitude-time distribution of the anomaly of (a) SST, (b) SSS, and (c) surface chlorophyll averaged between 5°S and 5°N. The black contour encloses the region with surface chlorophyll lower than 0.1 mg m^{-3}. Vertical lines indicate the zonal boundaries of the Niño3 (150°W, 90°W) and Niño4 (160°E, 150°W) regions. Regions with dots in (b) indicate normalized SSS errors larger than 0.80.

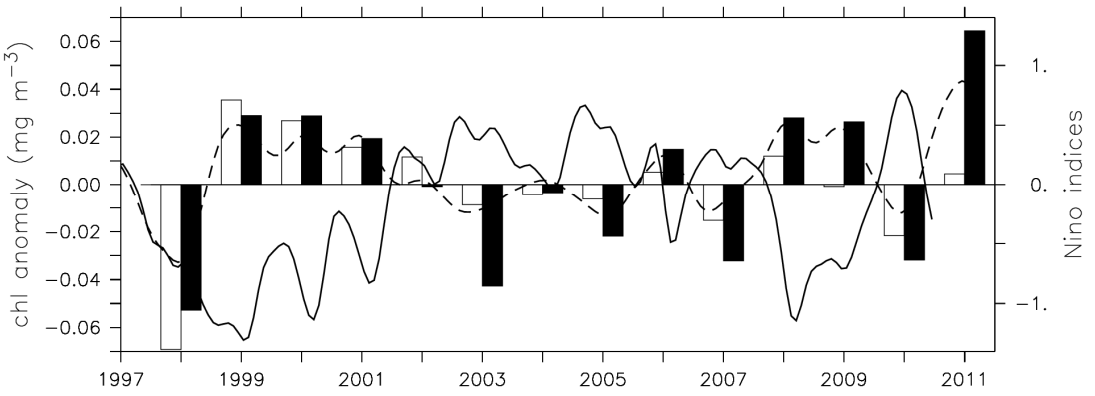

Figure 3. Surface chlorophyll anomaly averaged between September and February in the Niño3 (150°W-90°W, 5°S-5°N; hollow bars) and Niño4 (160°E-150°W, 5°S-5°N; filled bars) regions. EMI (full line) and 0.25×SOI (dashed line) are scaled on the right axis.

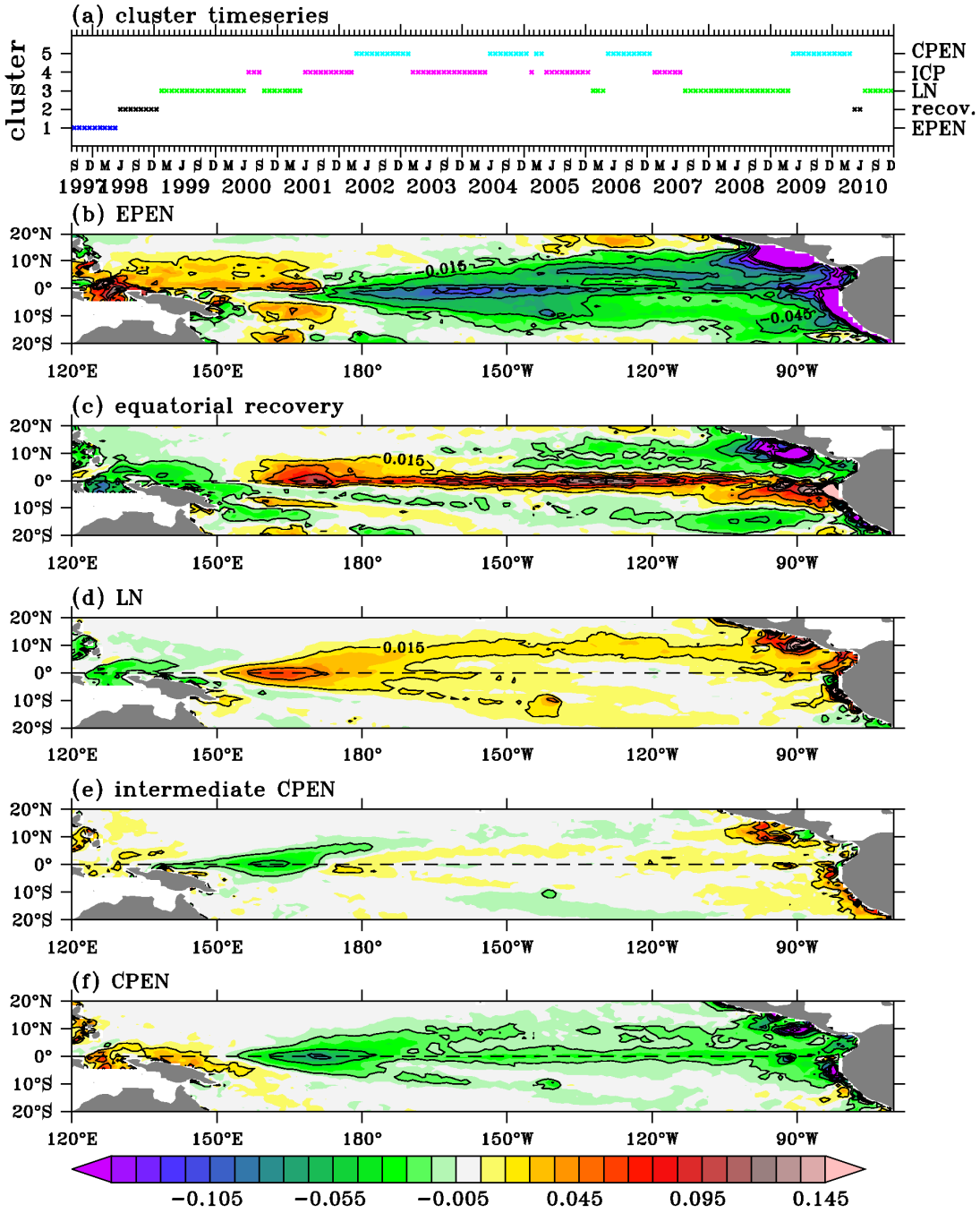

Figure 4. (a) Time series of the cluster analysis. Spatial patterns of the corresponding surface chlorophyll anomaly during the so-called (b) Eastern Pacific El Niño (EPEN), (c) equatorial recovery conditions (recov), (d) La Niña (LN), (e) intermediate Central Pacific period (ICP), and (f) Central Pacific El Niño (CPEN). Chlorophyll anomaly contours are every 0.03 mg m^{-3}. The 0 mg m^{-3} contour is omitted.

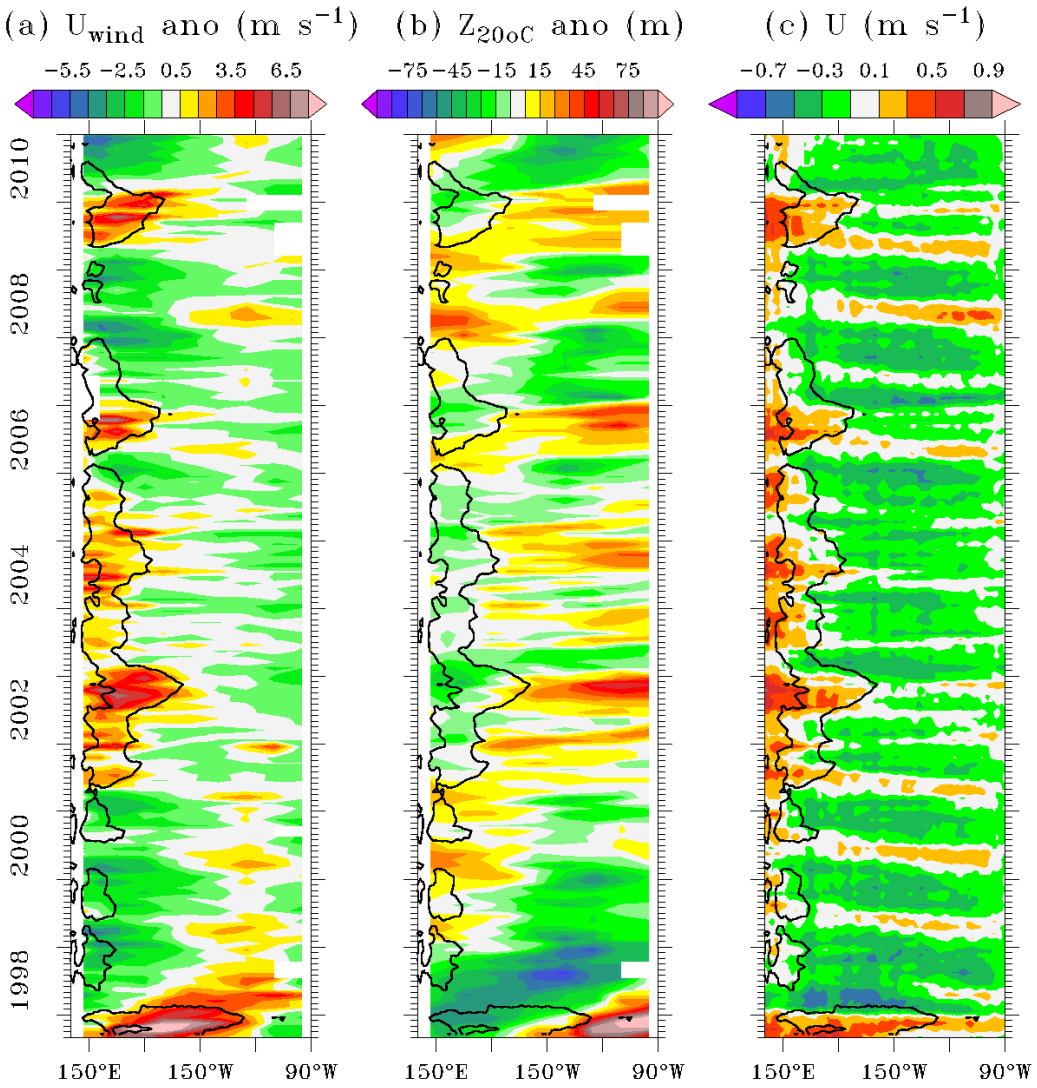

24 **Figure 5**. Longitude-time distribution along the equator of (a) zonal wind speed anomaly
25 (positive eastwards; colors; m s^{-1}), (b) 20°C isotherm depth anomaly (positive downward; m),
26 and (c) zonal surface current (positive eastwards; m s^{-1}). The black contours in (a-c) enclose
27 the region with surface chlorophyll lower than 0.1 mg m^{-3}.
28

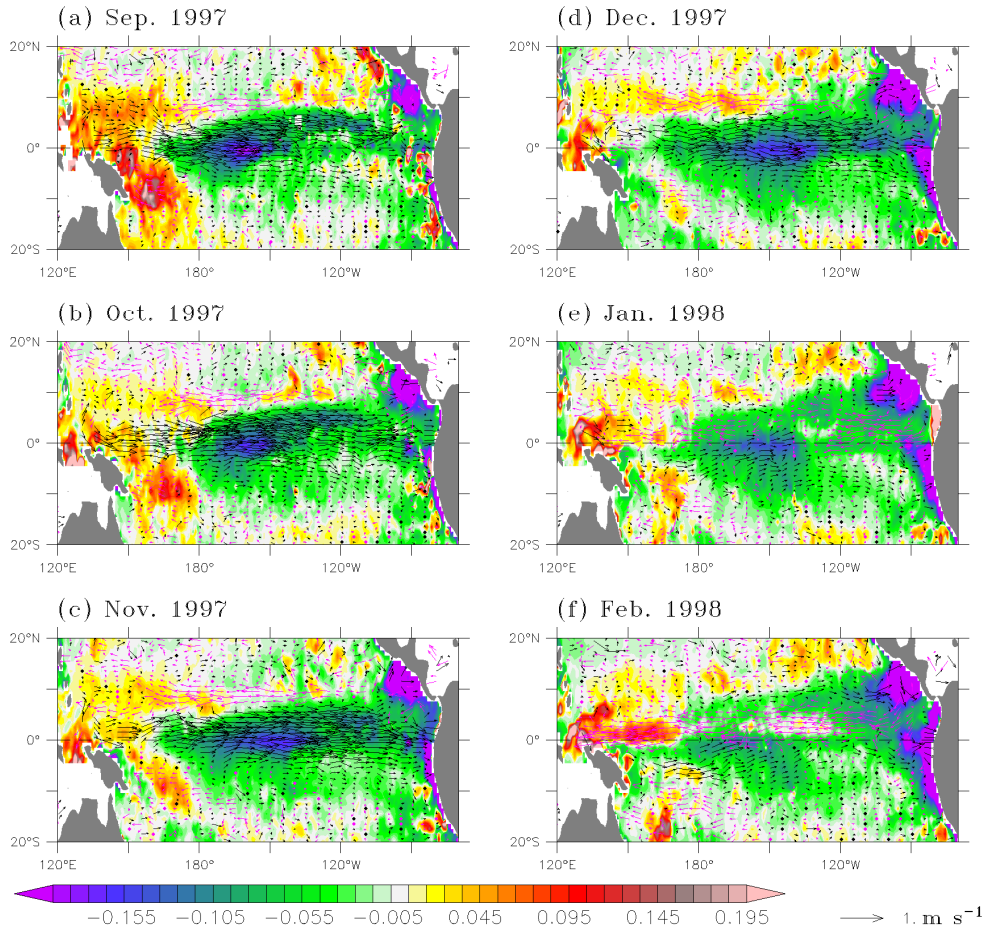

29 **Figure 6**. Maps of monthly surface chlorophyll anomaly (colors; mg m^{-3}) and surface layer

30 current anomaly (vectors; m s^{-1}) during the 1997-1998 Eastern Pacific El Niño. Current

31 vectors with eastward (westward) zonal component are in black (purple).

32

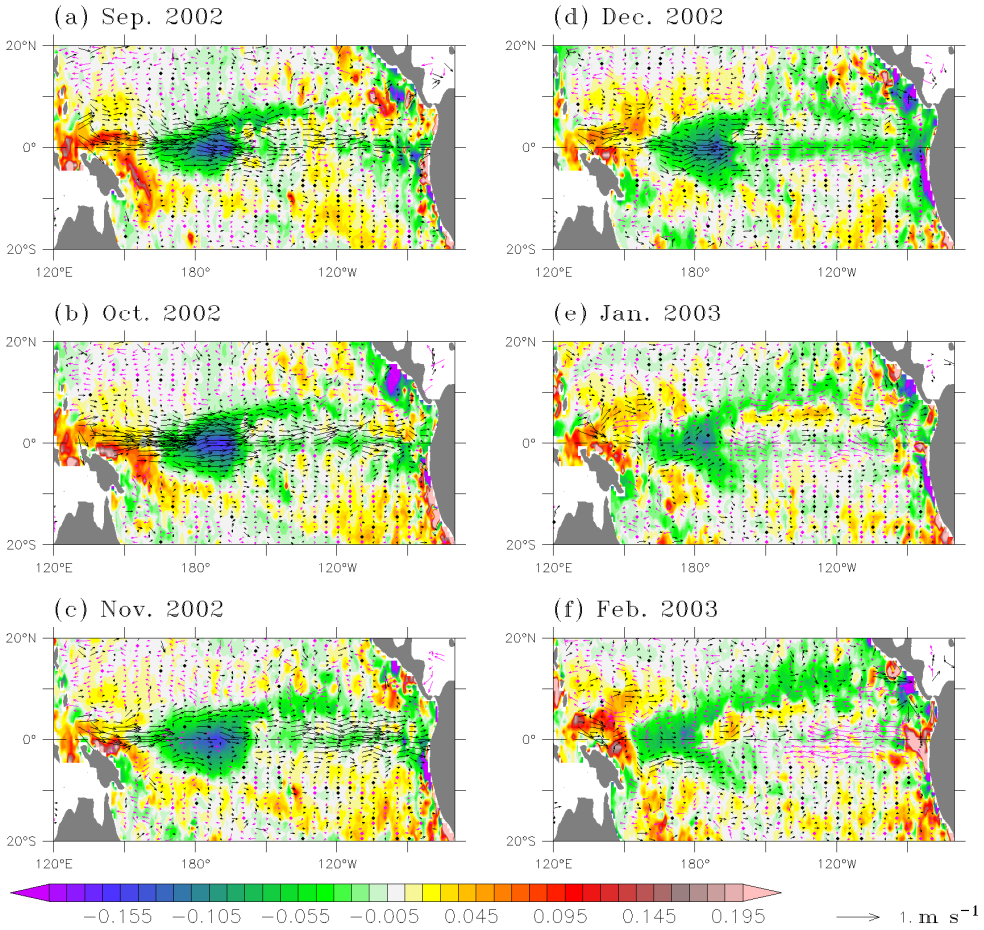

33 **Figure 7**. Maps of monthly surface chlorophyll anomaly (colors; mg m^{-3}) and surface layer

34 current anomaly (vectors; m s^{-1}) during the 2002-2003 Central Pacific El Niño. Current

35 vectors with eastward (westward) zonal component are in black (purple).

36

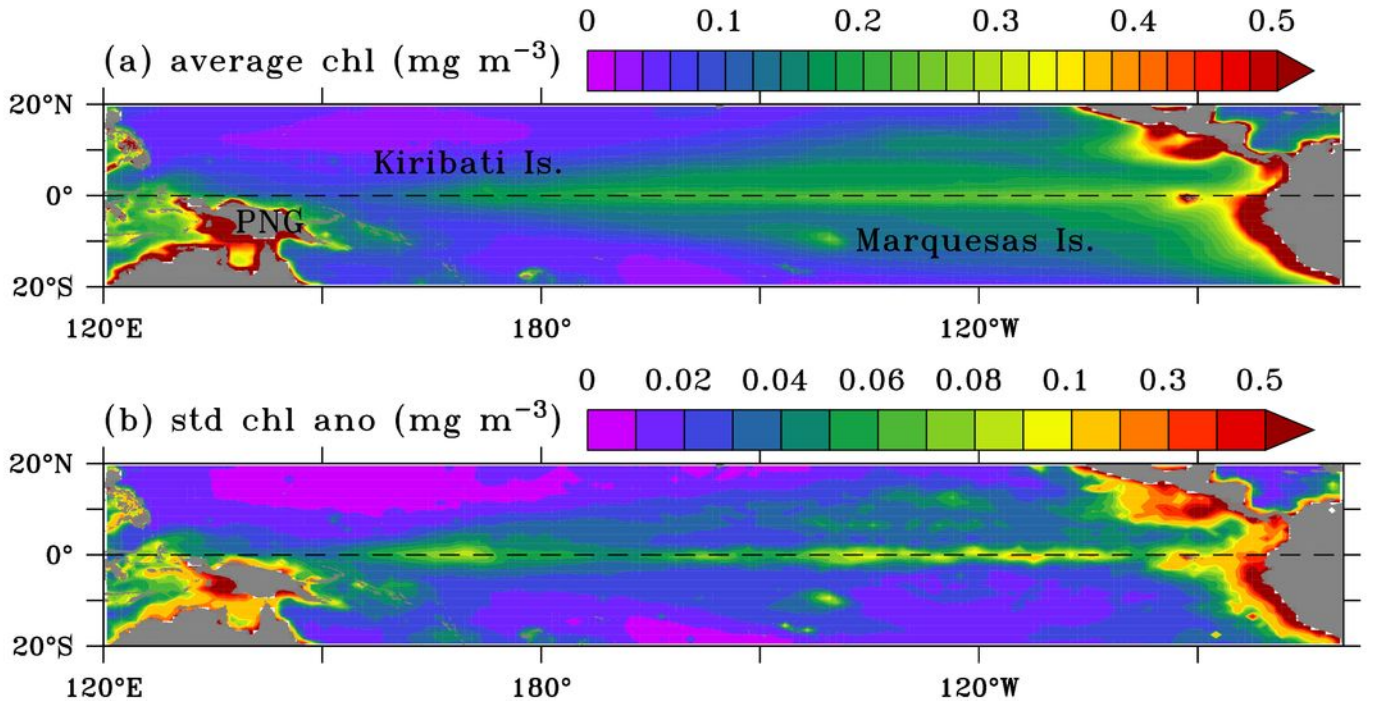
(a) average chl (mg m^{-3})
0
0.1
0.2
0.3
0.4
0.5
20°N
0°
20°S
Kiribati Is.
PNG
Marquesas Is.
120°E
180°
120°W
(b) std chl ano (mg m^{-3})
0
0.02
0.04
0.06
0.08
0.1
0.3
0.5
20°N
0°
20°S
120°E
180°
120°W

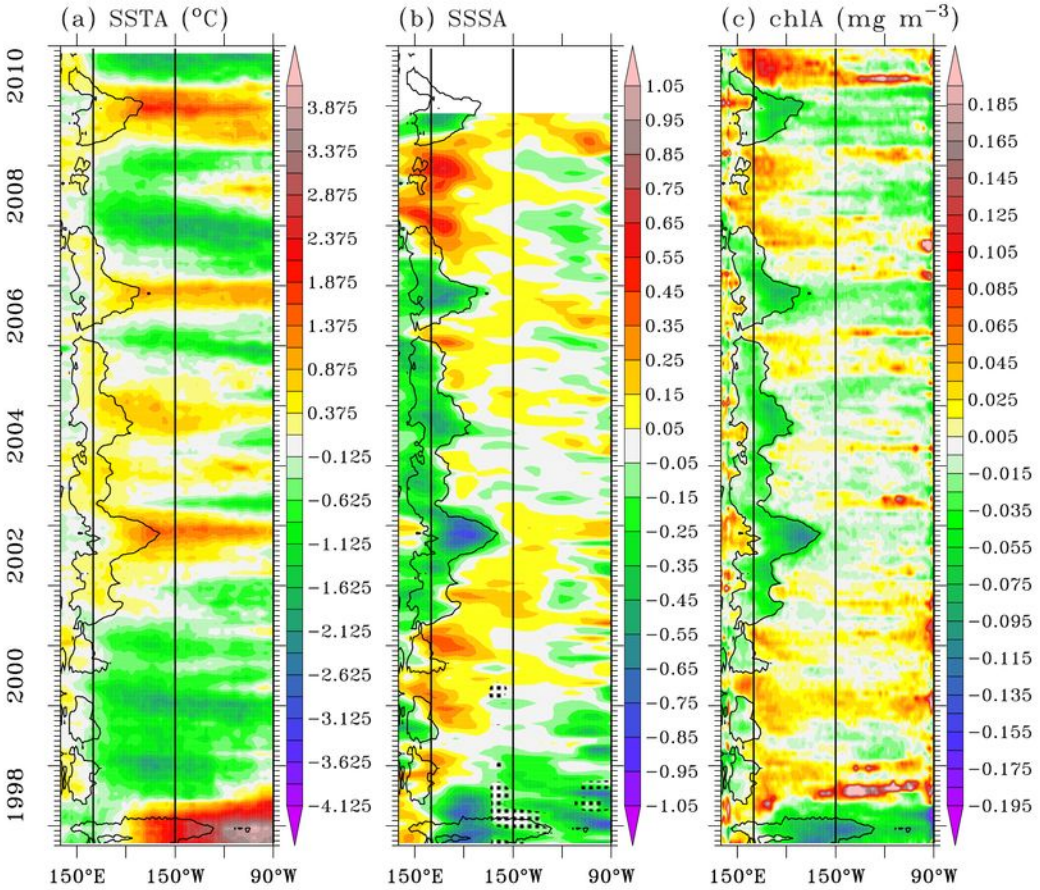
(a) SSTA (°C)
(b) SSSA
(c) chlA (mg m^{-3})
2010
2008
2006
2004
2002
2000
1998
3.875
3.375
2.875
2.375
1.875
1.375
0.875
0.375
−0.125
−0.625
−1.125
−1.625
−2.125
−2.625
−3.125
−3.625
−4.125
1.05
0.95
0.85
0.75
0.65
0.55
0.45
0.35
0.25
0.15
0.05
−0.05
−0.15
−0.25
−0.35
−0.45
−0.55
−0.65
−0.75
−0.85
−0.95
−1.05
0.185
0.165
0.145
0.125
0.105
0.085
0.065
0.045
0.025
0.005
−0.015
−0.035
−0.055
−0.075
−0.095
−0.115
−0.135
−0.155
−0.175
−0.195
150°E
150°W
90°W
150°E
150°W
90°W
150°E
150°W
90°W

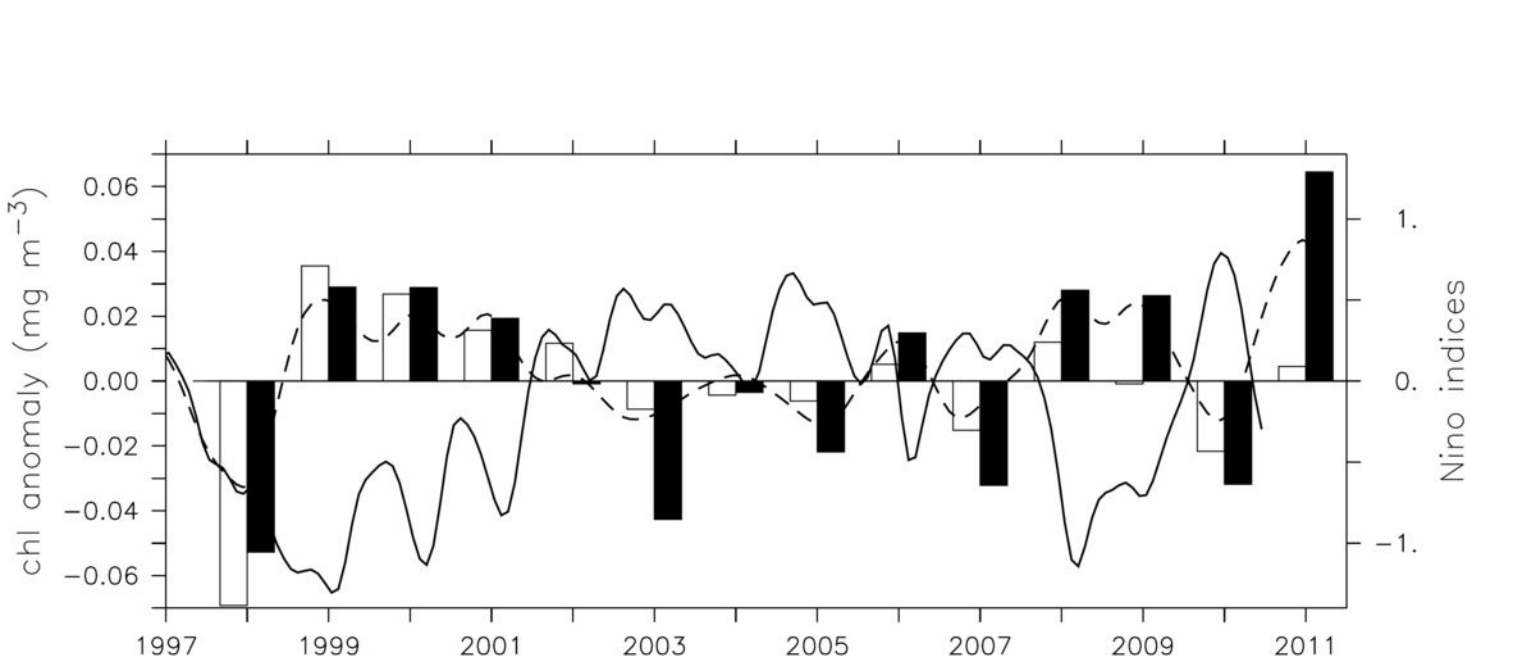
chl anomaly (mg m^{-3})
0.06
0.04
0.02
0.00
−0.02
−0.04
−0.06
1997
1999
2001
2003
2005
2007
2009
2011
Nino indices
1.
0.
−1.

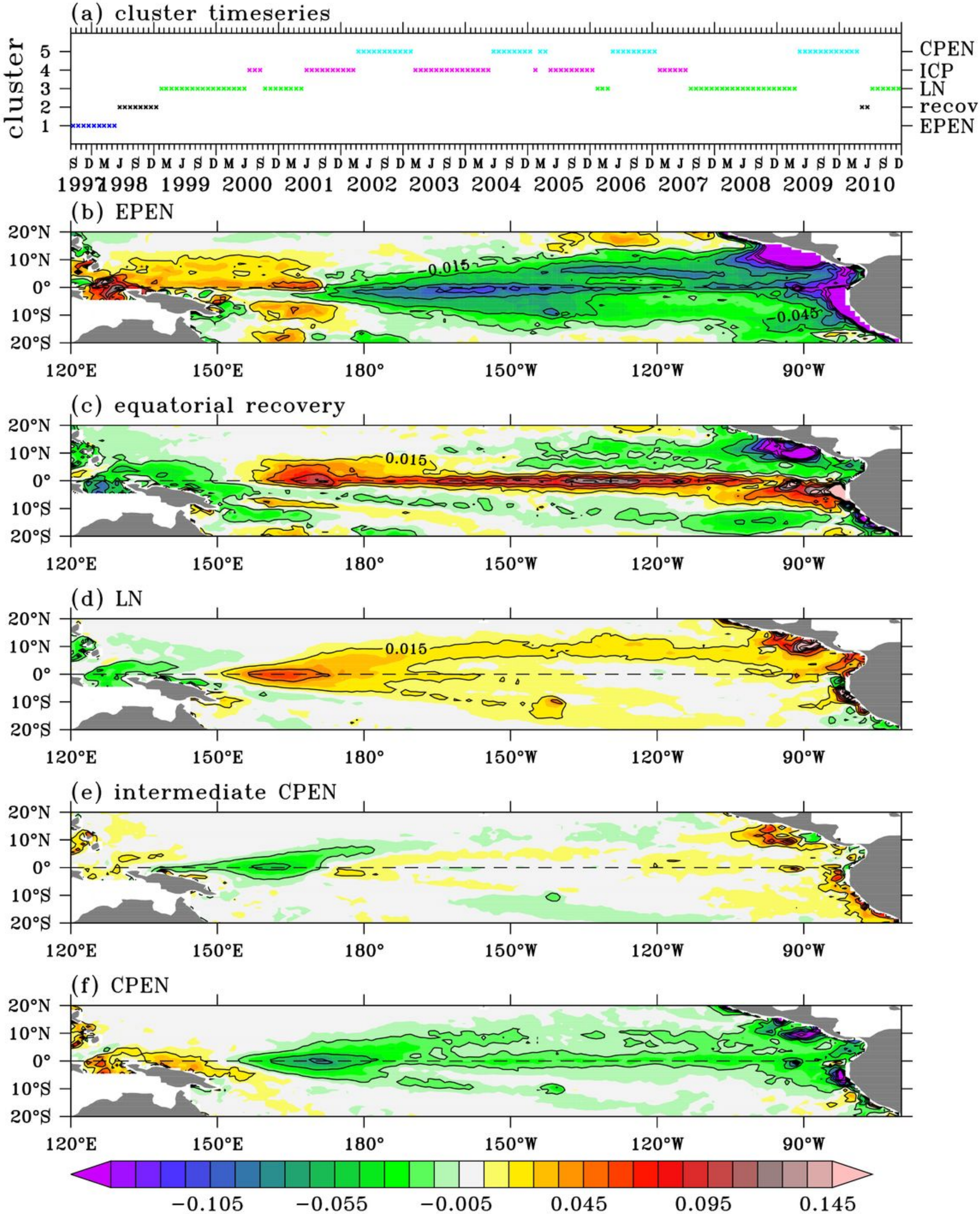
(a) cluster timeseries
cluster
1
2
3
4
5
CPEN
ICP
LN
recov.
EPEN
S D M J S D M J S D M J S D M J S D M J S D M J S D M J S D M J S D M J S D M J S D M J S D M J S D M J S D M J S D
1997 1998 1999 2000 2001 2002 2003 2004 2005 2006 2007 2008 2009 2010
(b) EPEN
-0.015
-0.045
(c) equatorial recovery
0.015
(d) LN
0.015
(e) intermediate CPEN
(f) CPEN
20°N
10°N
0°
10°S
20°S
120°E 150°E 180° 150°W 120°W 90°W
−0.105 −0.055 −0.005 0.045 0.095 0.145

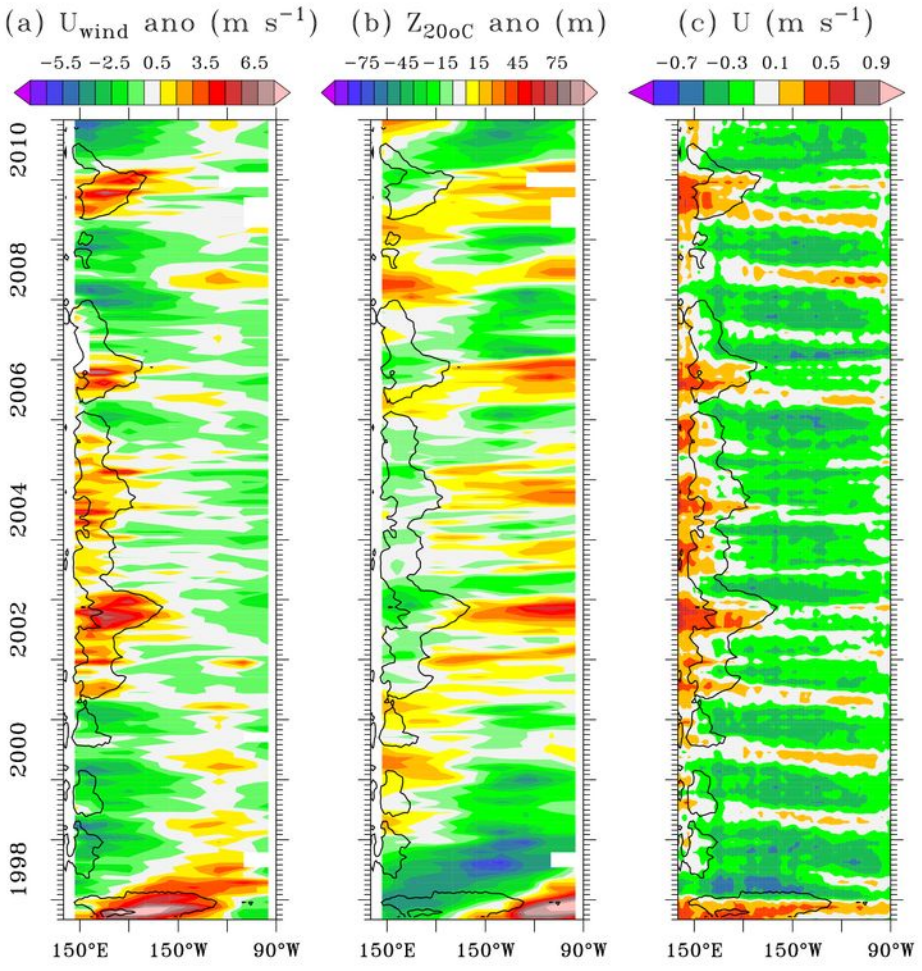
(a) U_{wind} ano (m s^{-1})
−5.5 −2.5 0.5 3.5 6.5
(b) Z_{20oC} ano (m)
−75 −45 −15 15 45 75
(c) U (m s^{-1})
−0.7 −0.3 0.1 0.5 0.9
2010
2008
2006
2004
2002
2000
1998
150°E
150°W
90°W

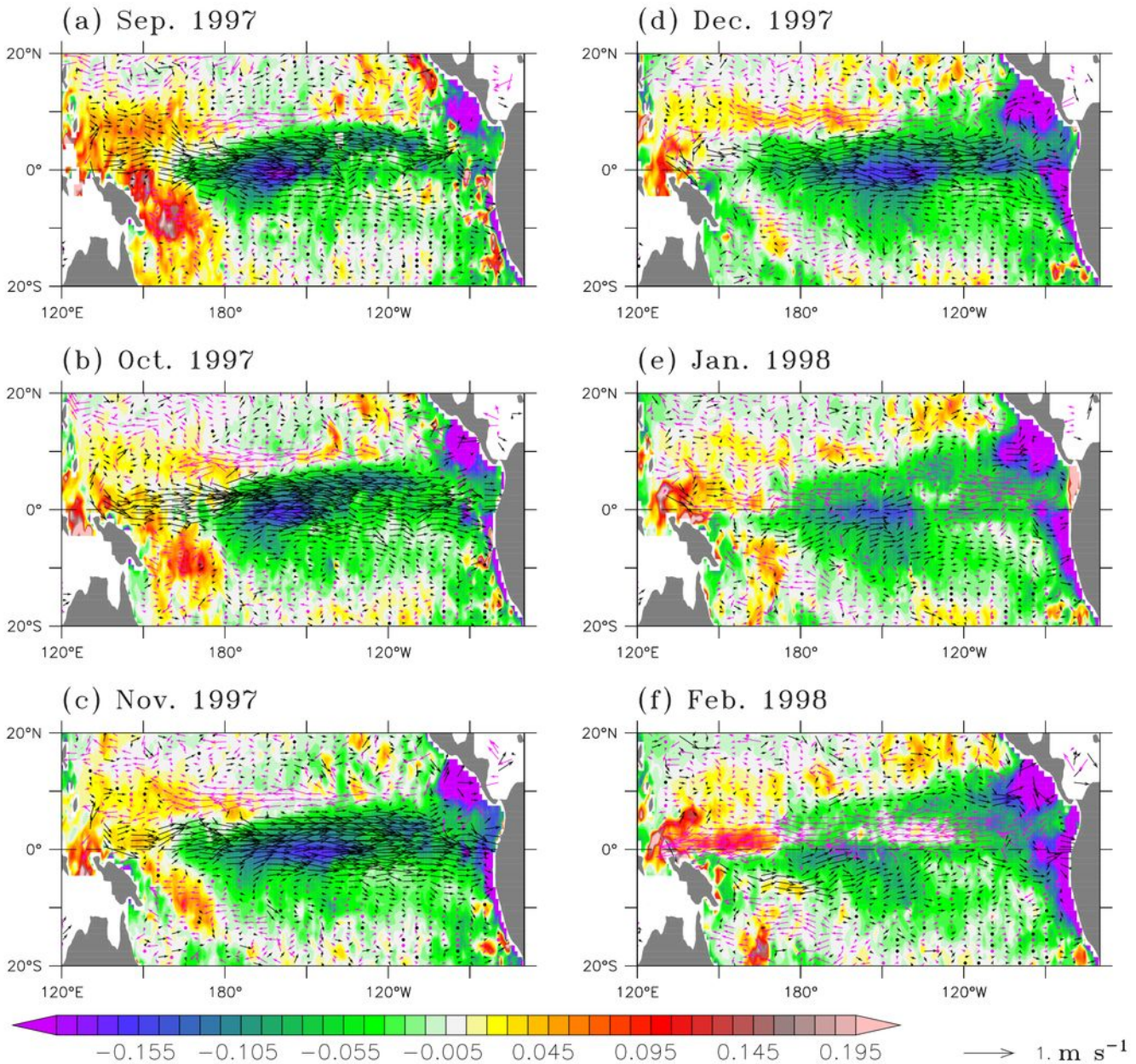
(a) Sep. 1997
(d) Dec. 1997
(b) Oct. 1997
(e) Jan. 1998
(c) Nov. 1997
(f) Feb. 1998
20°N
0°
20°S
120°E
180°
120°W
−0.155 −0.105 −0.055 −0.005 0.045 0.095 0.145 0.195
1. m s^{-1}

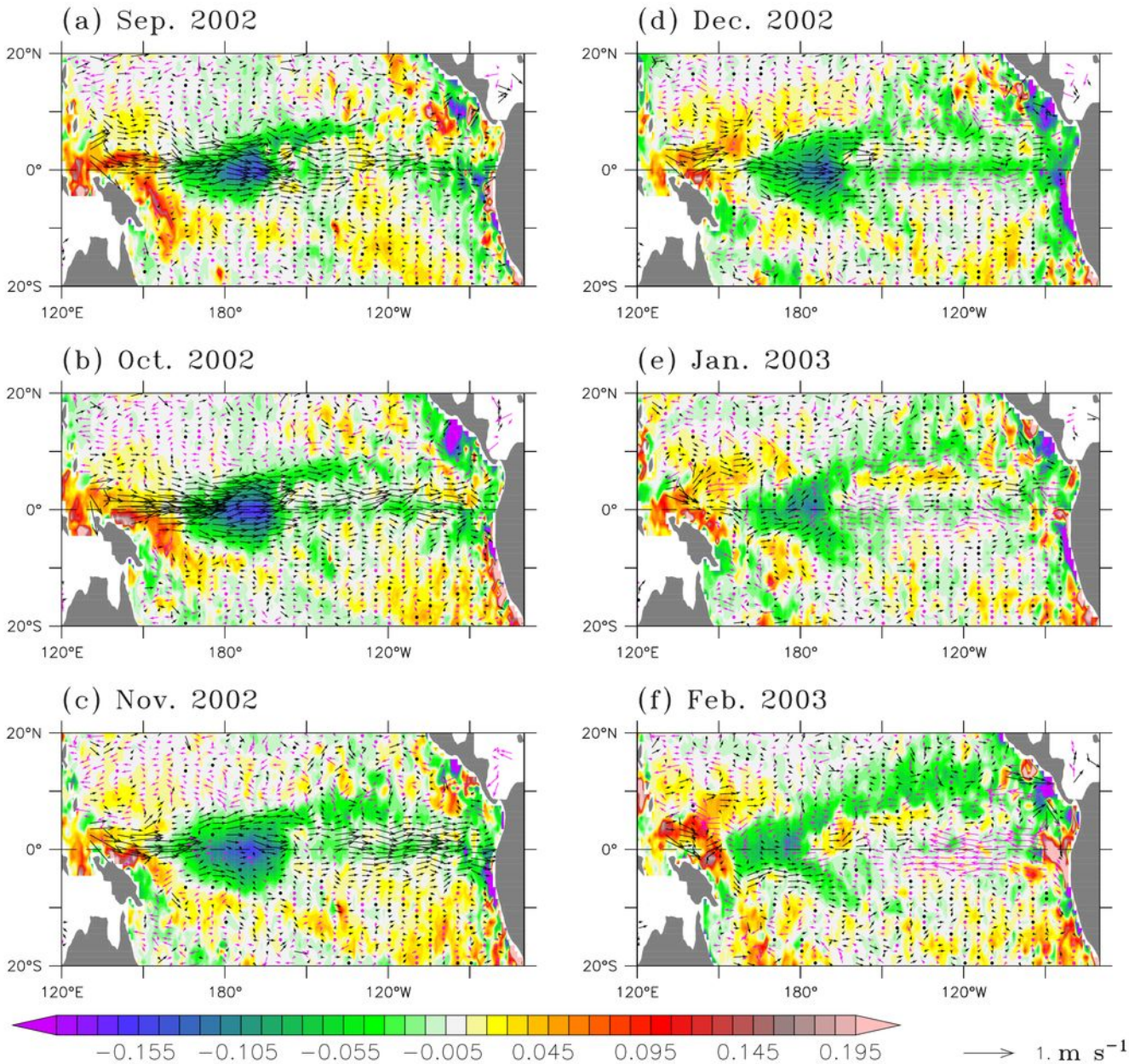
(a) Sep. 2002
(d) Dec. 2002
(b) Oct. 2002
(e) Jan. 2003
(c) Nov. 2002
(f) Feb. 2003
20°N
0°
20°S
120°E
180°
120°W
−0.155 −0.105 −0.055 −0.005 0.045 0.095 0.145 0.195
1. m s−1